European Journal of Medicinal Chemistry 46 (2011) 3590–3607

Contents lists available at ScienceDirect

European Journal of Medicinal Chemistry

journal homepage: http://www.elsevier.com/locate/ejmech

Original article

Synthesis and biological activity of tricyclic cycloalkylimidazo-, pyrimido- and diazepinopurinediones

Anna Drabczyńska [a], Olga Yuzlenko [a], Meryem Köse [b], Minka Paskaleva [b], Anke C. Schiedel [b], Janina Karolak-Wojciechowska [c], Jadwiga Handzlik [a], Tadeusz Karcz [a], Kamil Kuder [a], Christa E. Müller [b], Katarzyna Kieć-Kononowicz [a,*]

[a] Jagiellonian University Medical College, Faculty of Pharmacy, Department of Technology and Biotechnology of Drugs, Medyczna 9, PL 30-688 Kraków, Poland
[b] PharmaCenter Bonn, Pharmaceutical Institute, Pharmaceutical Chemistry I, University of Bonn, An der Immenburg 4, D-53121 Bonn, Germany
[c] Institute of General and Ecological Chemistry, Technical University of Łódź, Żwirki 36, PL 90-924 Łódź, Poland

ARTICLE INFO

Article history:
Received 26 October 2010
Received in revised form
10 May 2011
Accepted 10 May 2011
Available online 23 May 2011

Keywords:
Adenosine A_1 and A_{2A} receptor antagonists
Tricyclic xanthine derivatives
Cycloalkyl-1,3-diazepino[2,1-*f*]purinediones

ABSTRACT

Syntheses and physicochemical properties of N-cycloalkyl-substituted imidazo-, pyrimido- and 1,3-diazepino[2,1-*f*]purinediones are described. These derivatives were synthesized by cyclization of 7-halogenoalkyl-8-bromo-1,3-dimethylxanthine derivatives with aminocycloalkanes. The obtained compounds (**1**–**33**) were evaluated for their affinity to rat adenosine A_1 and A_{2A} receptors. Selected compounds were additionally investigated for affinity to the human A_1, A_{2A}, A_{2B} and A_3 receptor subtypes. The results of the radioligand binding assays at adenosine A_1 and A_{2A} receptors showed that most of the compounds exhibited adenosine A_{2A} receptor affinity at micromolar or submicromolar concentrations; an annelated pyrimidine ring was beneficial for A_{2A} affinity. The most potent A_{2A} ligands of the present series were compounds **6** (K_i 0.33 μM rat A_{2A}, 0.31 μM human A_{2A}), **8** (K_i 0.98 μM rat A_{2A}, 0.42 μM human A_{2A}) and **15** (K_i 0.24 μM rat A_{2A}, 0.61 μM human A_{2A}) with the latter one showing high A_{2A} selectivity. In NaCl shift assay, **15** was shown to be an antagonist at A_{2A} receptors. This result was confirmed for the best compounds **6**, **8**, **15** in cAMP accumulation studies. A 3D-QSAR equation with a good predicting power ($q^2 = 0.88$) for A_{2A} AR affinity was obtained. The compounds were evaluated in vivo as anticonvulsants in MES and ScMet tests and examined for neurotoxicity in mice (i.p.). Most of them showed anticonvulsant activity in chemically induced seizures; among them the diazepinopurinediones were the best (e.g. **31**) showing protection in both tests on short time symptoms, without signs of neurotoxicity. Five compounds, **8**, **17**, **20**, **29**, and **31**, exhibited anticonvulsant activity after peroral application in rats. Structure–activity relationships are discussed including the analysis of lipophilic and spatial properties. The new compounds, which contain a basic nitrogen atom and can therefore be protonated, may be good starting points for obtaining A_{2A} antagonists with good water-solubility.

1. Introduction

The adenosine receptor (AR) family consists of four subtypes: A_1, A_{2A}, A_{2B} and A_3 [1]. The responses of these four ARs are mediated by receptor-coupled G proteins, which may activate several different effector systems including adenylate cyclase, potassium and calcium channels, phospholipase A2 or C, and guanylate cyclase. Recent studies indicate a widening role for adenosine receptors in many therapeutic areas, including immunology, the cardiovascular system, and various CNS-mediated events such as sleep, neuroprotection, and pain [1–7].

Adenosine A_1 receptors are particularly ubiquitous within the central nervous system (CNS), with high levels being expressed in many regions of the brain. The distribution of adenosine A_{2A} receptors is more restricted, comprising lymphocytes, platelets, specific brain areas (striatum, nucleus accumbens, olfactory tubercle), vascular smooth muscle and endothelium [8].

Selective A_1 AR antagonists have demonstrated promising therapeutic potential for the treatment of cognitive diseases, renal failure, Alzheimer's disease and cardiac failure [9]. Adenosine A_{2A} receptor antagonists may be useful for the treatment of acute and chronic neurodegenerative disorders such as cerebral ischemia, Parkinson's, Huntington's, and Alzheimer's disease, as drugs controlling motor functions and exhibiting neuroprotective properties [10–18].

* Corresponding author. Tel: +48 12 6205581; fax: +48 12 6205596.
E-mail address: mfkonono@cyf-kr.edu.pl (K. Kieć-Kononowicz).

0223-5234/$ – see front matter © 2011 Elsevier Masson SAS. All rights reserved.
doi:10.1016/j.ejmech.2011.05.023

Since ARs offer an attractive target for drug development a number of studies have been carried out in order to find subtype-selective AR antagonists 2[19] especially in the group of xanthine derivatives [20]. Among A_1 antagonists with a xanthine structure the most potent ligands were in the group of 1,3-dipropyl-substituted derivatives bearing bulky residues in position 8 of the xanthine core (e.g. compound **1** [21] and KW-3902 [2]), whereas active A_{2A} AR antagonists were found among 8-styrylxanthines (e.g. MSX-2 [22,23], KW-6002 [22–26]) (Fig. 1). Furthermore, non-xanthine AR antagonists have been developed [19]. A major problem with adenosine receptor antagonists has been their generally low water-solubility [9,18,20].

Our groups have made considerable efforts to develop new selective xanthine adenosine receptor ligands. Our main focus was the investigation of tricyclic xanthine derivatives [27–32]. The most active A_1 AR ligands were found among 1,3-dipropyl-substituted benzylpyrimidopurinediones [31], while A_{2A} adenosine receptor ligands were mostly 1,3-dimethyl-substituted aryl- [30] and phenalkylpyrimidopurinediones [32].

As a continuation of our studies on tricyclic annelated purinediones the systematic examination of imidazo-, pyrimido- and diazepinopurinediones with cycloalkyl substituents was performed. Four elements in the target compounds were varied (Fig. 2): the size of the annelated ring (imidazo, pyrimido, diazepino), the size of the cycloalkyl moiety (from 3- to 8-membered), the spacer (from 0 to 2 C atoms), and the substituents (CH_3, OH, $OCOCH_3$) in the cycloalkyl ring.

Syntheses, structure elucidation by means of X-ray analysis, physicochemical properties, and in vitro evaluation of the potency at ARs, and in vivo examination of anticonvulsant properties were performed.

2. Chemistry

The synthesis of 1,3-dimethylperhydroimidazo-, -pyrimido- and -1,3-diazepino[2,1-*f*]purinediones with cycloalkyl substituents in the N-8, N-9 or N-10 position, respectively, of the annelated ring was accomplished as shown in Fig. 3.

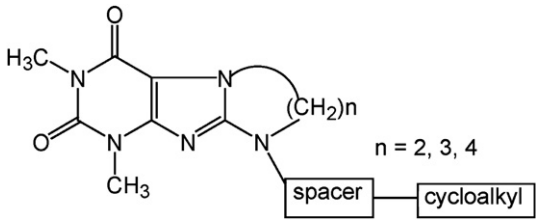

Fig. 2. General structure of the tricyclic xanthine ligands with N-cycloalkyl substituents.

The following starting materials were used, which were obtained according to described procedures [30,33,34]: 7-(2-bromoethyl)-8-bromotheophylline, 7-(3-chloropropyl)-8-bromotheophylline and 7-(4-bromobutyl)-8-bromotheophylline. These were cyclized with amines under various reaction conditions with regard to the amount of amine, solvent and reaction time.

The data are summarized in Table 1. Compounds **3** and **11** were described previously [35], but no biological activity has been reported. The structures of the synthesized compounds were confirmed by UV, IR and ^{1}H NMR spectra: UV spectra showed a bathochromic shift typical for 8-aminoxanthine derivatives with λ_{max} of about 300 nm [36]. The IR absorption bands were typical of xanthine derivatives [37] and in the ^{1}H NMR spectra, the expected chemical shifts were observed. All compounds were purified by recrystallization.

3. X-ray structure analysis

It is well known that hydrogen bonds are very important among all intermolecular interactions [38–42]. They are responsible for molecular recognition and/or self-organization of the molecules [43]. The H-bonds take part in the formation of complexes between

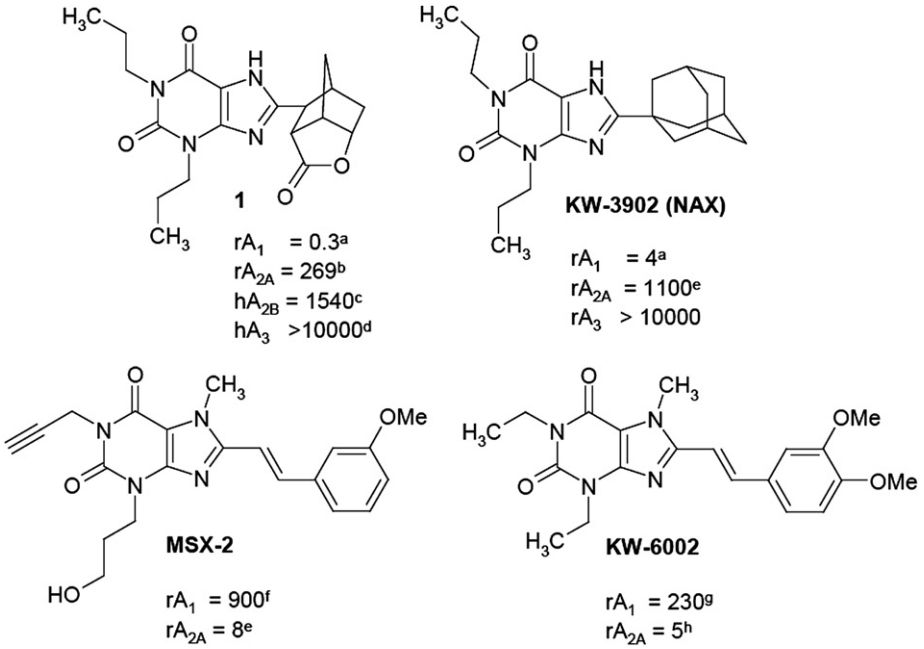

Fig. 1. Potent and selective xanthine adenosine A_1 and A_{2A} receptor antagonists. K_i values are given in nM. [a]Radioligand [^{3}H]CPX, rat brain cortex membranes; [b]radioligand [^{125}I]ZM 241385, rat brain striatum membranes; [c]radioligand [^{3}H]MRS 1754, HEK 293 cells expressing human A_{2B} AR; [d]radioligand [^{125}I]AB-MECA, HEK 293 cells expressing human A_3 AR; [e]radioligand [^{3}H]CGS21680, rat brain striatal membranes; [f]radioligand [^{3}H]CHA, rat brain cortical membranes; [g]radioligand [^{3}H]CCPA, rat brain cortical membranes; [h]radioligand [^{3}H]MSX-2, rat brain striatal membranes.

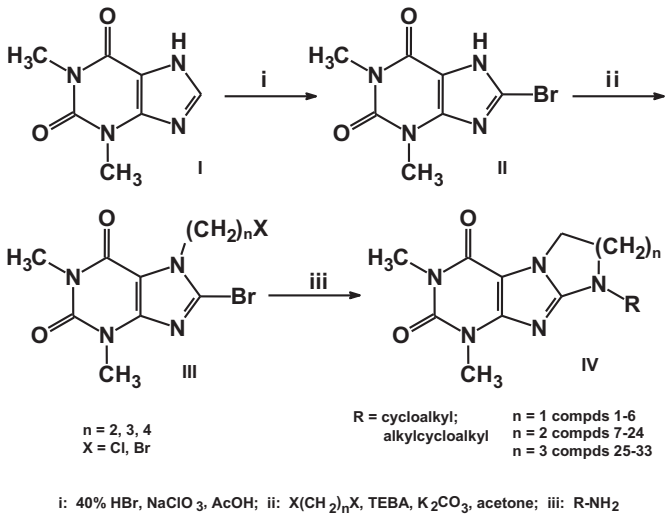

Fig. 3. Synthesis of imidazo-, pyrimido- and 1,3-diazepino[2,1-*f*]purinediones.

biological receptors and their ligands and they are responsible for packing motif formation in nearly all crystals of organic substances. The most important information about H-bond geometry and topology can be taken from crystallographic data. Therefore, X-ray structure analysis of small, biologically active molecules is highly useful. Previous X-ray studies on imidazo-, pyrimido- and 1,3-diazepino[2,1-*f*]purinediones with various aromatic substituents in the N-8, N-9 or N-10 position respectively, have suggested that C–H···O=C interactions are crucial for crystal structure architecture [27–32]. Such H-bonds were mainly formed between the O2 purine oxygen atom and protons from the annelated rings. It should be noted that aromatic groups at the nitrogen atom participated only incidentally in structural motif formation, usually via their substituents (for example OCH_3) [31]. Recently, among derivatives with various cycloalkyl substituents at N-8, N-9 or N-10 (Fig. 2), monocrystals of three compounds – **7**, **13** and **33** – were selected for X-ray structure analysis (Fig. 4). These comprise the smallest 3-membered (**7**) and the largest 8-membered cykloalkyl derivative (**33**).

In the studied structures the bicyclic xanthine moiety is planar. Annelated pyrimidone rings in **7** and **13** are half-chairs, while the diazepine ring in **33** adopts a boat conformation. Superimposition

Table 1
Physical data and reaction conditions of N-cycloalkylimidazo-, pyrimido-, and diazepino[2,1-*f*]purinediones.

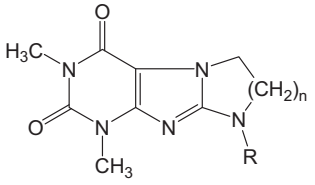

Compound	R	*n*	Formula, MW	M.p. (°C)	Yield of cyclization (%)	Reaction medium (excess of amine)	Reaction time [h] reflux	Crystal. solvent	TLC R_f eluent
1	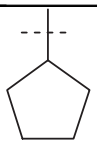	1	$C_{14}H_{19}N_5O_2$, 289.33	167–169	46	Xylene (5)	10	Ethanol	0.30[a]
2	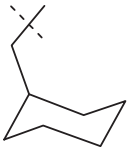	1	$C_{16}H_{23}N_5O_2$, 317.37	201–203	63	Butanol (5)	10	Ethanol	0.55[a]
3	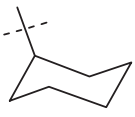	1	[35]						
4	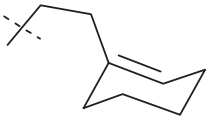	1	$C_{17}H_{23}N_5O_2$, 329.39	162–164	53	Xylene (4)	6	Methanol	0.49[a]
5	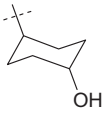 cis trans	1	$C_{15}H_{21}N_5O_3 \cdot H_2O$, 337.37	215–218	40	– (20)	10	50% Ethanol	0.35[b]

Table 1 (*continued*)

Compound	R	*n*	Formula, MW	M.p. (°C)	Yield of cyclization (%)	Reaction medium (excess of amine)	Reaction time [h] reflux	Crystal. solvent	TLC R_f eluent
6	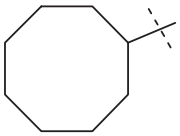	1	$C_{17}H_{25}N_5O_2$, 331.41	153–155	68	Xylene (5)	10	Ethanol	0.42[a]
7		2	$C_{13}H_{17}N_5O_2$, 275.31	220–221	69	Butanol (5)	10	50% Ethanol	0.50[a]
8		2	$C_{14}H_{19}N_5O_2$, 289.33	183–185	59	Me-Digol (2)	5	70% Ethanol	0.57[a]
9	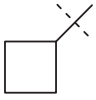	2	$C_{14}H_{19}N_5O_2$, 289.33	251–253	48	Me-Digol (2)	10	Ethanol	0.51[a]
10	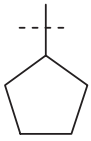	2	$C_{15}H_{21}N_5O_2$, 303.36	234–236	82	Me-Digol (2)	5	Ethanol	
11	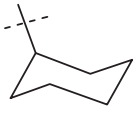	2	[35]						
12	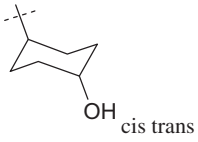	2	$C_{16}H_{23}N_5O_3$, 333.38	231–233	83	– (20)	5	20% Ethanol	0.11[a]
13	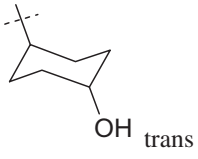	2	$C_{16}H_{23}N_5O_3$, 333.38	262–264	62	Me-Digol (2)	5	Methoxyethanol	0.11[a]
14	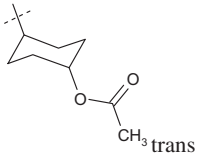	2	$C_{18}H_{25}N_5O_4$, 357.42	305–306	79	Acetic anhydride (10)	5	Methoxyethanol	0.53[a]
15	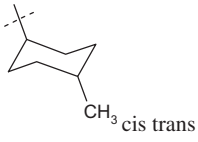	2	$C_{17}H_{25}N_5O_2$, 331.41	182–184	63	Butanol (3)	10	50% Ethanol	0.55[a]

(*continued on next page*)

Table 1 (*continued*)

Compound	R	*n*	Formula, MW	M.p. (°C)	Yield of cyclization (%)	Reaction medium (excess of amine)	Reaction time [h] reflux	Crystal. solvent	TLC R_f eluent
16	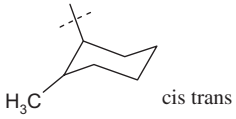	2	$C_{17}H_{25}N_5O_2$, 331.41	172–174	95	Butanol (5)	10	Ethanol/H_2O	0.55[a]
17	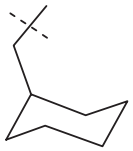	2	$C_{17}H_{25}N_5O_2$, 331.41	178–180	94	Me-Digol (2)	5	70% Ethanol	0.57[a]
18	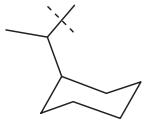	2	$C_{18}H_{27}N_5O_2 \cdot ½H_2O$, 354.44	148–149		[c]		ethanol	0.60[a]
19	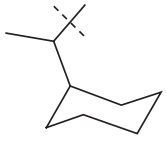	2	$C_{18}H_{27}N_5O_2 \cdot ½H_2O$, 354.44	149–151	69	DMF (2)	5	50% Ethanol	0.60[a]
20	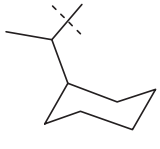	2	$C_{18}H_{27}N_5O_2 \cdot ½H_2O$, 354.41	149–150	65	DMF (2)	5	50% Ethanol	0.60[a]
21	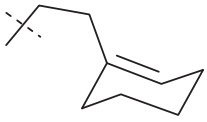	2	$C_{18}H_{25}N_5O_2$, 343.42	162–164	62	DMF (2)	8	Ethanol/H_2O	0.56[a]
22	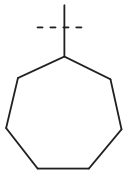	2	$C_{17}H_{25}N_5O_2$, 331.41	200–202	51	Me-Digol (2)	10	Ethanol	0.57[a]
23	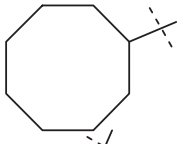	2	$C_{18}H_{27}N_5O_2$, 345.44	186–188	84	Me-Digol (2)	5	70% Ethanol	0.52[a]
24	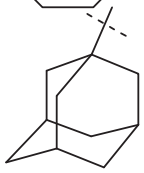	2	$C_{20}H_{25}N_5O_2$, 367.44	293–295	62	Me-Digol (2)	8	Methoxyethanol	0.60[a]
25	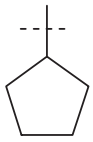	3	$C_{16}H_{23}N_5O_2$, 317.38	182–184	79	DMF (5)	10	Ethanol	0.68[a]

Table 1 (*continued*)

Compound	R	*n*	Formula, MW	M.p. (°C)	Yield of cyclization (%)	Reaction medium (excess of amine)	Reaction time [h] reflux	Crystal. solvent	TLC R_f eluent
26	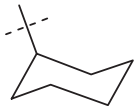	3	$C_{17}H_{25}N_5O_2$, 331.47	228–230	55	DMF (5)	10	Ethanol	0.59[a]
27	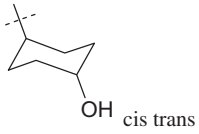	3	$C_{17}H_{25}N_5O$, 347.41	233–235	62	–(20)	5	30% Ethanol	0.77[d]
28	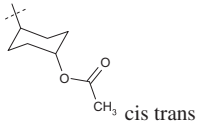	3	$C_{19}H_{27}N_5O_4$, 389.45	137–140	82	Acetyl anhydride (10)	5	50% Ethanol	0.69[a]
29	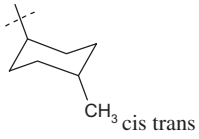	3	$C_{18}H_{27}N_5O_2$, 345.44	212–214	74	Butanol (5)	10	Ethanol/H_2O	0.66[a]
30	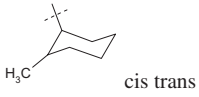	3	$C_{13}H_{27}N_5O_2$, 345.44	214–217	89	Butanol (5)	10	Ethanol	0.67[a]
31	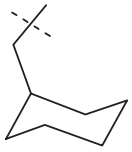	3	$C_{18}H_{27}N_5O_2$, 345.44	133–134	80	DMF (4)	10	Methanol/H_2O	0.65[a]
32	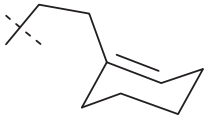	3	$C_{19}H_{27}N_5O_2$, 357.45	113–115	91	DMF (4)	8	Methanol	0.62[a]
33	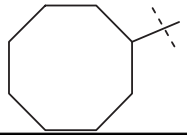	3	$C_{19}H_{29}N_5O_2$, 359.46	164–165	56	DMF (5)	10	Ethanol/H_2O	0.46[e]

Me-Digol – diethylene glycol monomethyl ether.
[a] Benzene/acetone – 7:3.
[b] Butanol/butyl acetate/$CHCl_3$ – 5:1:1.
[c] Stoichiometric mixture of **19** and **20**.
[d] Benzene/acetone/methanol – 1:1:1.
[e] Hexane/dioxane – 5:2.

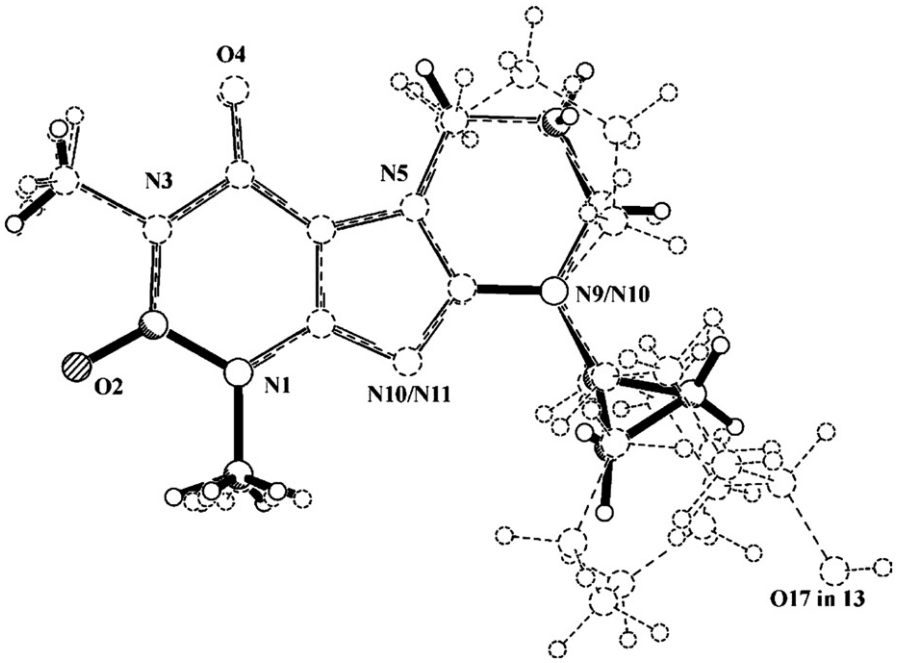

Fig. 4. Superimposition of **7**, **13** and **33** (molecule A) with respect to the bicyclic xanthine moieties.

of all three structures (Fig. 4) shows that the cycloalkyl residues are oriented in a similar mode – *trans* with respect to the N9–(or N10–)C12 bond. In the third structure (**13**) – cyclohexyl-substituted – the hydroxyl group is positioned *trans* with respect to the N9–C12 bond. In that prominent localization, OH seems to be an evident H-bond partner.

As it often happens for conformationally flexible groups, pyrimidone in **13**, and diazepine and cyclooctyl in **33** show a conformational disorder in the structure. This is evident in the structure of **33** with three molecules in a crystallographically independent unit, designated A (atom numbering without indices), B (with indices ′) and C (with indices ″ and # for disordered atoms). Two of them (A and B) differ insignificantly in the cyclooctyl conformation (Fig. 5). The third one, with disordered diazepine and cyclooctyl (both with s.o.f. = 0.5), consists in fact of two identical molecules which are mirror images (Fig. 5).

The structure of the crystals for three studied compounds is based on C–H···O=C hydrogen bonds. In **7** and **13**, two C–H···O2 interactions (where one carbon is from pyrimidone and the other from cycloalkyl) join molecules into a ribbon (Fig. 6 and Tables in Supplementary data). The C7–H···O4 bond is forming a connection resulting in two ribbons which form the main structural motif in the structure of **7** and **13**. The cyclohexyl-OH substituent in **13** has been the origin of strong H-bonds which join the molecules along the *c*-axis [O17–H···O17(x,1/2 − y,1/2 + z) = 2.856 Å]. As a consequence between the double ribbons there is enough space for a methanol molecule which is located in the canal down the *c*-axis. Solvent molecules form a H-bonding chain, similar to the one observed for the drug molecules. Even if C–H···O=C hydrogen bonds are also identified in **33**, the main structural motif is based on stacked bicycles of three independent molecules (Fig. 6). These molecules form a sandwich of A and B with C in between. In the sequence A···C···B distances between bicycles equal 3.56 Å and 5.58 Å, respectively. The main motifs form a column down the *c*-axis with a distance between sandwiches of 3.60 Å. Nevertheless, H-bonds of C–H···O (Table in Supplementary data) are responsible for the molecules position. All six oxygen atoms are proton acceptors, while protons mainly come from the azepine ring carbons. Columns

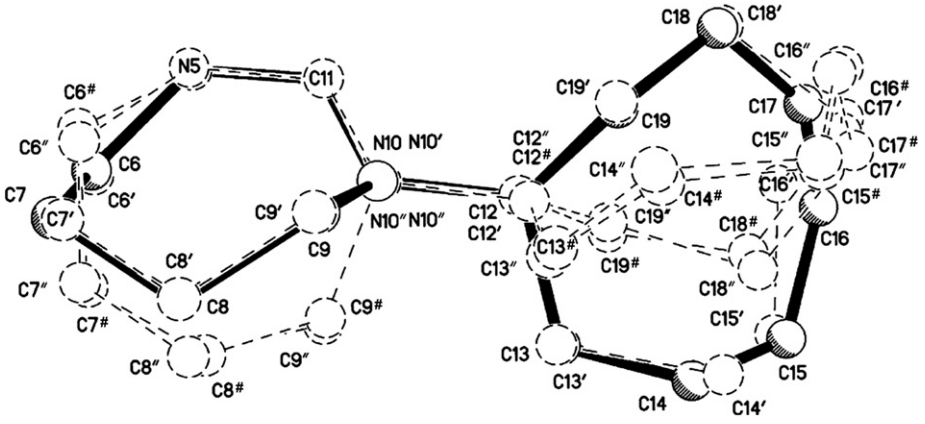

Fig. 5. Superimposition of diazepine and cyclooctyl residues from the structure of **33**.

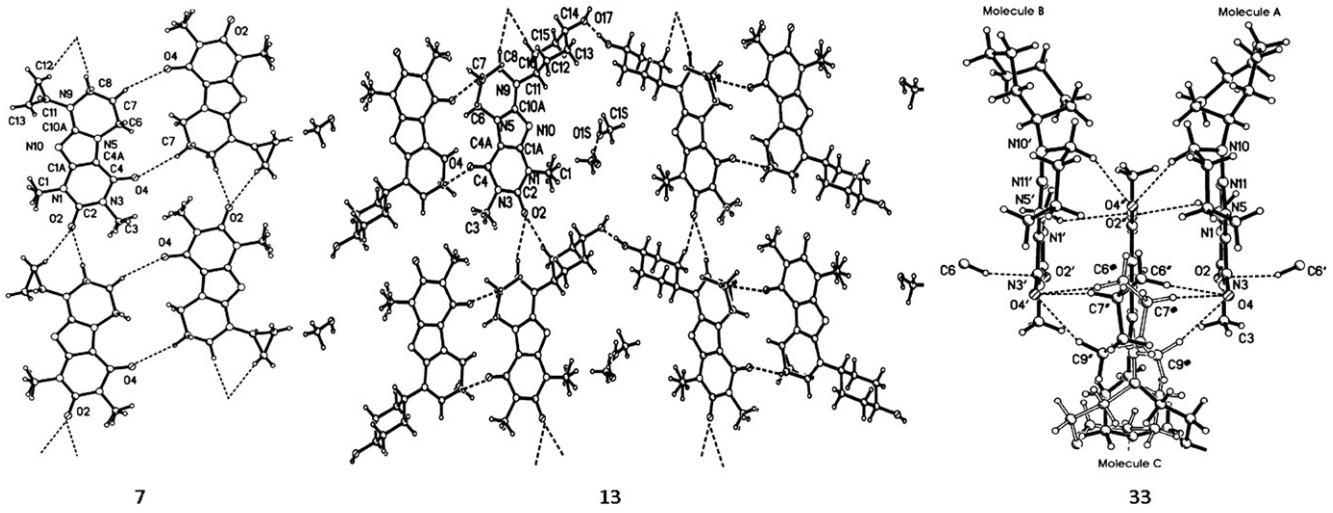

Fig. 6. Main structural motifs in the structures of **7**, **13** and **33**.

are getting together through the weak H-bonds of the cyclooctyl carbon hydrogen atoms C13″—H···O2″ ($-0.5+x,1.5-y,z$) = 3.625 Å.

X-ray structure analysis of pyrimido- and 1,3-diazepino[2,1-*f*] purinediones with various cycloalkyl substituents in the N-9 or N-10 position respectively, confirmed our earlier observation that both oxygen atoms, O2 and O4, can be competent H-bond acceptors. Moreover in the studied compounds carbon atoms from cycloalkyl substituents may serve as additional proton-donating centers.

4. Pharmacology

All compounds were tested in vitro in radioligand binding assays for affinity to A_1 and A_{2A} ARs at rat cortical membrane and rat striatal membrane preparations, respectively. Selected compounds were further tested for their affinity to human A_1, A_{2A}, A_{2B} and A_3 receptors recombinantly expressed in CHO cells. As A_1 AR radioligand [^{3}H]2-chloro-N^6-cyclopentyladenosine ([^{3}H]CCPA) [44] was used and as A_{2A} radioligand [^{3}H]1-propargyl-3-(3-hydroxypropyl)-7-methyl-8-(*m*-methoxystyryl)xanthine ([^{3}H]MSX-2) was applied [45]; [^{3}H]4-(2-[7-amino-2-(2-furyl-[1,2,4]-triazolo[2,3-*a*]-[1,3,5]-triazin-5ylamino] ethyl)phenol ([^{3}H]ZM241385) [46] and [^{3}H]8-(4-(4-(4-chlorophenyl) piperazine-1-sulfonyl)phenyl)-1-propylxanthine ([^{3}H]PSB-603) [47] were used as radioligands in A_{2B} binding studies and [^{3}H]2-phenyl-8-ethyl-4-methyl-(8*R*)-4,5,7,8-tetrahydro-1*H*-imidazo[2,1-*i*]purine-5-one ([^{3}H]PSB-11) was used as A_3 adenosine selective receptor ligand [48]. The results are presented in Tables 2 and 3. The potent A_{2A} antagonist KW-6002 and the non-selective ligand caffeine were included for comparison. Sodium chloride shift experiments [49,50] were performed for one of the most potent and A_{2A}-selective compounds of the present series in order to confirm that the N-cycloalkyl-substituted tricyclic purinediones are antagonists at the A_{2A} ARs (Fig. 7). Furthermore, some compounds were investigated in functional cAMP accumulation studies. Thus, the most potent compounds were investigated for their potency to inhibit cAMP accumulation induced by the agonist NECA in CHO cells expressing the human A_{2A} receptor.

The compounds were additionally evaluated in vivo as anticonvulsants by the Antiepileptic Drug Development Program (ADD) of the National Institute of Neurological Disorders and Stroke (NINDS) in Bethesda according to the Antiepileptic Screening Project (ASP) [52,53]. Phase I of the evaluation included three tests, maximal electroshock (MES), subcutaneous pentylentetrazol (ScMet) and the rotorod test for neurological toxicity (TOX) performed in mice. The MES assays have predictive value for agents as potential therapeutics in the management of grand mal epilepsy, whereas the ScMet test is for those likely to be effective against petit mal [52,53]. Minimal motor impairment was measured by the rotorod toxicity test. The results are given in Table 4.

Some compounds were administered orally to rats and examined in the MES, ScMet screen and rotorod tests. For two compounds (**17**, **31**) a quantitative test was performed and ED_{50} values were determined. Results of this test were compared with literature data available for valproate [54] as reported in Table 5.

4.1. In vitro tests

The results of the radioligand binding assays at adenosine A_1 and A_{2A} receptors (Table 2) showed that N-cycloalkylpurinediones (with the exception of: **4**, **26**, **31**, **32**, which were non-selective) exhibited affinity to A_{2A} receptors but poor A_1 affinity. It was noticed that for both imidazo- and diazepinopurinediones substituted with a cyclohex-1-enylethyl moiety (**4**, **32**) selectivity was lost, while for pyrimidopurinedione with the same substituent (**21**) high selectivity (>40) was maintained. Adamantyl derivative **24** was inactive at both ARs subtypes. A decisive influence on A_{2A} affinity had the size of the annelated ring. As observed previously [30] also in this series of compounds, the pyrimidine ring was beneficial for A_{2A} affinity. Decrease to 5-membered (compounds **1**–**6**) or enlargement to 7-membered rings (compounds **25**–**33**) led to a reduction in adenosine receptor affinity (only two compounds, **6** and **29**, showed submicromolar affinity).

The size of the cycloalkyl moiety had a smaller influence on A_{2A} affinity, however bigger rings were favourable (larger than 5 C, but no cycloheptyl). Introducing a 1–2 carbon atom linker between the cycloalkyl moiety and the annelated ring increased affinity (compare the affinity of compounds **2** and **3**, **7** and **8**, **11** and **17** or **21**). The influence of substituents, OH or CH_3, in the cyclohexyl ring was interesting: a methyl group was beneficial only in position 4 producing the best ligand of the present series, compound **15** ($K_i = 0.24$ μM). The configuration of the OH substituent was crucial for the affinity to the adenosine A_{2A} receptor. The mixture of *cis* and *trans* isomers of 4-hydroxycyclohexyl derivative **12** was more potent than the *trans*-isomer **13** alone, which indicates the preference of the A_{2A} receptor for the *cis*-configuration. The *S*-configuration of the optically active compounds **19** (*R*) and **20** (*S*) was favourable increasing affinity to the A_{2A} receptor to the submicromolar range (compound **20**).

Table 2
Affinities of cycloalkylimidazo-, pyrimido-, and diazepino[2,1-*f*]purinediones at adenosine A_1 and A_{2A} receptors.

Compound		Adenosine A_1 receptor (rat brain cortical membranes) vs. [^{3}H]CCPA $K_i \pm$ SEM (μM) (% inhibition ± SEM at 25 μM or 10 μM, respectively) ($n = 3$)	Adenosine A_{2A} receptor (rat brain striatal membranes) vs. [^{3}H]MSX-2 $K_i \pm$ SEM (μM) (% inhibition ± SEM at 25 μM) ($n = 3$)	A_{2A} AR selectivity A_1/A_{2A}
KW-6002 [29] (Fig. 1)		0.230 ± 0.030	0.00515 ± 0.00025	45
Caffeine [29]		18.8 ± 5.6	32.8 ± 8.0	0.6
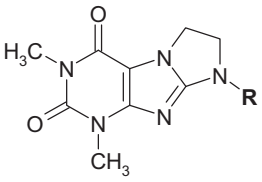				
Imidazopurinediones				
1	Cyclopentyl	ca. 25 (50 ± 3%)	3.10 ± 1.18	~8
2	Cyclohexylmethyl	≥25 (41 ± 2%)	2.00 ± 0.70	≥13
3	Cyclohexyl	>10 (27 ± 4% at 10 μM)	2.58 ± 0.68	>4
4	Cyclohex-1-enylethyl	2.45 ± 0.18	2.02 ± 0.05	1
5	4-Hydroxycyclohexyl	>25 (4 ± 3%)	4.48 ± 0.41	>6
6	Cyclooctyl	≥25 (40 ± 2%)	0.33 ± 0.09	≥76
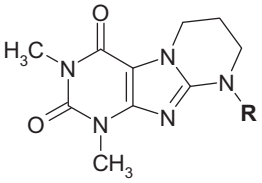				
Pyrimidopurinediones				
7	Cyclopropyl	≥25 (43 ± 6%)	1.24 ± 0.33	ca. 20
8	Cyclopropylmethyl	2.39 ± 0.58	0.98 ± 0.24	2
9	Cyclobutyl	≥10 (39 ± 3%)	1.93 ± 0.37	≥5
10	Cyclopentyl	5.31 ± 1.29	1.00 ± 0.45	5
11	Cyclohexyl	≥25 (39 ± 3%)	0.81 ± 0.01	≥31
12	4-Hydroxycyclohexyl	>25 (8 ± 3%)	2.04 ± 0.18	>12
13	*trans*-4-Hydroxycyclohexyl	>10 (11 ± 5%)	3.63 ± 0.25	>3
14	4-Acetocyclohexyl	>10 (5 ± 5%)	6.20 ± 0.62	>2
15	4-Methylcyclohexyl	≥25 (38 ± 1%)	0.24 ± 0.15	≥100
16	2-Methylcyclohexyl	>25 (31 ± 3%)	1.08 ± 0.26	>23
17	Cyclohexylmethyl	2.49 ± 0.35	0.61 ± 0.24	4
18	Cyclohexylethyl	7.58 ± 0.54	1.24 ± 0.04	6
19	(*R*)-Cyclohexylethyl	7.89 ± 0.14	1.30 ± 0.10	6
20	(*S*)-Cyclohexylethyl	11.9 ± 1.38	0.887 ± 0.053	13
21	Cyclohex-1-enylethyl	14.7 ± 1.76	0.50 ± 0.18	44
22	Cycloheptyl	>10 (4 ± 2%)	2.67 ± 0.71	4
23	Cyclooctyl	≥25 (33 ± 1%)	0.57 ± 0.15	≥44
24	1-Adamantyl	>10 (7 ± 9%)	>10 (13 ± 11)	1
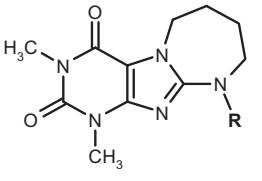				
Diazepinopurinediones				
25	Cyclopentyl	5.06 ± 0.64	1.38 ± 0.26	4
26	Cyclohexyl	2.13 ± 0.44	2.96 ± 1.20	1
27	4-Hydroxycyclohexyl	≥25 (44 ± 3%)	3.81 ± 0.09	~7
28	4-Acetocyclohexyl	4.87 ± 0.84	1.74 ± 0.85	3
29	4-Methylcyclohexyl	3.44 ± 0.98	0.83 ± 0.20	4
30	2-Methylcyclohexyl	>25 (27 ± 13%)	3.46 ± 1.81	>7
31	Cyclohexylmethyl	5.18 ± 1.15	3.5 ± 0.75	1
32	Cyclohex-1-enylethyl	1.66 ± 0.17	1.17 ± 0.13	1
33	Cyclooctyl	>10 (16 ± 9%)	6.86 ± 0.94	>1

Table 3
Affinities of selected compounds and standard antagonists at human adenosine A_1, A_{2A}, A_{2B} and A_3 receptors recombinantly expressed in CHO cells.

Compound		Adenosine A_1 receptor (human recombinant) vs. [^{3}H]CCPA $K_i \pm$ SEM [μM] (% inhibition ± SEM at 10 μM) ($n = 3$)	Adenosine A_{2A} receptor (human recombinant) vs. [^{3}H]MSX-2 $K_i \pm$ SEM [μM] (% inhibition ± SEM at 10 μM) ($n = 3$)	Adenosine A_{2B} receptor (human recombinant) vs. [^{3}H]ZM241385* vs. [^{3}H]PSB-603** $K_i \pm$ SEM [μM] (% inhibition ± SEM at 10 μM) ($n = 3$)	Adenosine A_3 receptor (human recombinant) vs. [^{3}H]PBS-11 $K_i \pm$ SEM [μM] (% inhibition ± SEM at 10 μM) ($n = 3$)
Caffeine		44.9 ± 6.2#	23.4 ± 7.1#	20.5 ± 2.2#	>100 [51]
KW-6002		2.07 ± 0.43#	0.0908 ± 0.0228#	≥10 (47 ± 2%)[a] [49]	4.47 ± 4.06#
Imidiazopurinediones					
3	Cyclohexyl	>10 (41 ± 4%)	1.61 ± 0.34	>10 (11 ± 7%)**	>10 (12 ± 6%)
5	4-Hydroxy-cyclohexyl	>10 (7 ± 3%)	3.27 ± 1.43	>10 (24 ± 24%)*	>10 (0 ± 0%)
6	Cyclooctyl	>10 (21 ± 9%)	0.306 ± 0.024	0.80 ± 0.16**	>10 (16 ± 2%)
Pyrimidopurinediones					
8	Cyclopropyl-methyl	7.13 ± 1.04	0.417 ± 0.199	12.5 ± 1.6*	>10 (1 ± 1%)
9	Cyclobutyl	10.3 ± 2.76	0.847 ± 0.650	>10 (21 ± 4%)**	>10 (5 ± 4%)
11	Cyclohexyl	>10 (37 ± 8%)	1.61 ± 0.41	>10 (0 ± 5%)**	>10 (12 ± 5%)
13	*trans*-4-Hydroxy-cyclohexyl	>10 (21 ± 2%)	19.0 ± 1.5	>10 (0 ± 4%)**	>10 (27 ± 5%)
14	4-Aceto-cyclohexyl	>10 (5 ± 3%)	21.9 ± 7.0	>10 (0 ± 10%)**	>10 (27 ± 9%)
15	4-Methyl-cyclohexyl	>10 (28 ± 4%)	0.61 ± 0.21	>10 (16 ± 16%)*	>10 (16 ± 6%)
21	Cyclohex-1-enylethyl	6.90 ± 1.34	0.933 ± 0.141	>10 (6 ± 4%)**	>10 (23 ± 3%)
22	Cycloheptyl	>10 (41 ± 5%)	1.16 ± 0.31	>10 (0 ± 18%)**	>10 (6 ± 1%)
23	Cyclooctyl	>10 (17 ± 15%)	1.53 ± 0.59	>10 (32 ± 0%)*	>10 (52 ± 5%)
24	1-Adamantyl	>10 (15 ± 2%)	>10 (0 ± 23%)	>10 (0 ± 3%)**	1.29 ± 0.30
Diazepinopurinediones					
28	4-Aceto-cyclohexyl	>10 (16 ± 7%)	>10 (8 ± 1%)	>10 (29 ± 1%)*	>10 (28 ± 6%)
33	Cyclooctyl	>10 (29 ± 3%)	2.40 ± 0.49	>10 (0 ± 6%)**	1.67 ± 0.22

[a] [^{3}H]PSB-298 was used as a radioligand [49].
* [^{3}H]ZM241385 [46].
** [^{3}H]PSB-603 [47].
# Ref. [18].

Several compounds were more potent at the rat as compared to the human A_{2A} receptor subtype: **13** and **28** (almost five-fold), **14**, **15** and **23** (about three-fold), **11** and **21** (two-fold) (Tables 2 and 3). While compound **6** was similarly potent in both species, some of the compounds showed higher affinity for the human as compared to the rat A_{2A} AR, including **3**, **5**, **8**, **9**, **22**, and **33** (up to three-fold). Affinity for A_1 AR, when it was observed, was as well worse for human AR (for **8**, **28**) as better for **21** (two times). Affinity to the human A_{2B} and A_3 receptor of selected compounds (**3**, **5**, **6**, **8**, **9**, **11**, **13**, **14**, **15**, **21**, **22**, **23**, **24**, **28**, and **33**) was very weak only cyclooctyl derivative **6** showed submicromolar affinity and cyclopropylmethyl derivative **8** exhibited micromolar affinity to the human A_{2B} AR. Compounds **24** and **33** were the only derivatives which displayed good, micromolar affinity for the human A_3 AR (K_i 1.29 and 1.67 μM, respectively) (Table 3). One of the most potent A_{2A}-selective ligands (compound **15**) was investigated for its functional properties using a sodium chloride shift assay. While the curve for the agonist NECA was significantly shifted to the right in the presence of 100 mM of sodium chloride, the curve for **15** was unaltered in the same experiment. This clearly indicates that **15** acts as an antagonist at A_{2A} receptors (Fig. 7). To confirm these results, the three most potent compounds **6**, **8**, **15** were evaluated in functional experiments. They were investigated for their potency to inhibit NECA-induced cAMP accumulation in CHO cells expressing the human A_{2A} receptor (Fig. 8). The compounds clearly behaved as competitive antagonists as the concentration–response curve of NECA was shifted to the right in a parallel fashion in their presence. K_b values determined in living CHO cells expressing the human adenosine A_{2A} receptor were well in accordance with K_i values determined in radioligand binding studies at membrane preparations of the same cell line. Owing to the structural similarity of all compounds in this series we suppose that they are all antagonists.

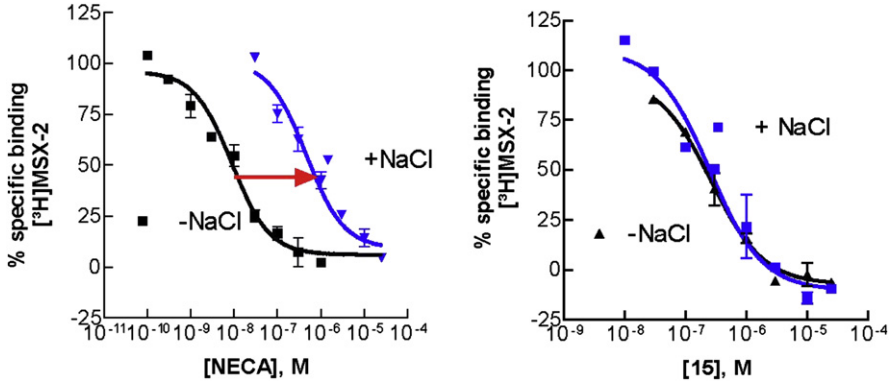

Fig. 7. Radioligand binding curves of the agonist N-ethylcarboxamidoadenosine (NECA) and of compound **15** at rat adenosine A_{2A} receptors in the absence and in the presence of NaCl (100 mM); IC_{50} NECA (−NaCl): 7.05 ± 0.70 nM, IC_{50} NECA (+NaCl): 366 ± 197 nM (49-fold shift); IC_{50} **15** (−NaCl): 263 ± 152 nM, IC_{50} **15** (+NaCl): 251 ± 19 nM.

Table 4
Anticonvulsant activity and neurotoxicity of cycloalkylimidazo-, pyrimido-, and 1,3-diazepino[2,1-*f*]purinediones (i.p., mice).

Compound[a]	MES[b,c]				ScMet[b,c]				Toxicity[b,c]				ASP[d] class
	0.25 h	0.5 h	1 h	4 h	0.25 h	0.5 h	1 h	4 h	0.25 h	0.5 h	1 h	4 h	
1	–	–	–	–	–	300 (4/5)	–	–	–	300 (2/4)	–	–	2
2	–	–	–	–	–	–	–	–	–	–	–	–	3
3	–	–	–	–	–	300 (1/1)	–	–	–	100 (1/8)	–	–	2
4	–	–	–	–	–	–	–		–	300 (1/4)	–	300 (1/2)	3
5	–	–	–	–	–	–	–	–	–	–	–	–	3
6	–	–	–	–	–	–	–	300 (2/5)[e]	–	–	–	–	2
7	–	–	–	–	–	–	–	–	–	300 (4/4)	–	–	3
8	100 (2/3)	300 (1/1)	–	–	–	100 (3/5)	–	–	–	300 (4/4)	–	–	1
9	–	–	–	–	–	–	–	–	–	–	–	–	3
10	–	–	–	–	–	300[f]	300 (3/5)	–	–	–	–	–	2
11	–	–	–	–	–	300 (4/5)	–	–	–	–	–	–	2
12	–	–	–	–	–	300 (4/5)[g]	–	–	–	–	–	–	2
13	–	–	–	–	–	300 (1/5)[e]	–	–	–	–	–	–	2
14	–	–	–	–	–	–	–	–	–	–	–	–	3
15	–	–	–	–	–	300 (3/5)	[g]	–	–	300 (1/4)	–	–	2
16	–	–	–	–	–	–	–	–	–	–	–	–	3
17	–	–	–	–	100 (3/5)	300 (5/5)	100 (1/5)	–	–	300 (1/4)	–	–	1
18	–	–	–	–	–	–	–	–	–	300 (1/4)	–	–	3
19	–	–	–	–	–	–	–	–	–	300 (1/4)	–	–	3
20	–	100 (1/3)	–	–	–	100 (1/5)	–	–	–	300 (1/4)	–	–	1
21	–	–	–	–	–	100 (1/5)	–	–	–	300 (1/4)	–	–	1
22	–	–	–	–	–	–	–	–	–	–	–	–	3
23	–	–	–	–	–	300 (5/5)	–	–	–	100 (1/8)	–	–	3
24	–	–	–	–	–	–	–	–	–	300 (1/4)	–	–	3
25	–	–	–	–	–	300 (1/5)	–		–	–	–	–	2
26	–	–	–	–	–	–	–	–	–	–	–	–	3
27	–	–	–	–	–	300 (1/1)	–	–	–	100 (1/8)	–	–	2
28	–	–	–	–	–	300 (5/5)	–	–	–	100 (2/8)	–	–	2
29	–	–	–	–	100 (3/5)	300 (5/5)	100 (3/5)	–	–	–	–	–	1
30	–	–	–	–	–	300 (2/5)	–	–	–	–	–	–	2
31	–	300 (1/1)	–	–	–	100 (4/5)	–	–	–	–	–	–	1
32	–	–	–	–	–	–	–	–	–	100 (1/8)	100 (1/4)	–	3
33	–	300 (1/5)[e]	–	–	–	–	–	–	–	100 (1/8)	–	–	2

The dash (–) indicates an absence of activity/toxicity at maximum dose administration (300 mg/kg).
[a] Administered as suspension in 0.5% methylcellulose.
[b] Doses of 30, 100, 300 mg/kg. The figures in the table indicate the minimum dose whereby activity was demonstrated. The animals were examined 0.5 and 4 h after injections were made. For compounds **8**, **17**, **29** the biological response was observed after 0.25 h.
[c] Meaning of figures in the anticonvulsant test: e.g. 1/5 means the number of animals protected/number of animals tested; in toxicity tests: number of animals that exhibited toxicity/number of animals tested.
[d] Classification is as follows: 1 – anticonvulsant activity at 100 mg/kg or less; 2 – anticonvulsant activity at 300 mg/kg; 3 – lack of anticonvulsant activity at 300 mg/kg.
[e] Myoclonic jerks.
[f] Death following clonic seizure.
[g] Death following tonic extension.

4.2. In vivo tests

Unsubstituted imidazo-, pyrimido-, and diazepinopurinediones did not show protective activity in both electric and chemical seizures [30]. Introduction of cycloalkyl substituents at the nitrogen atom of the annelated ring resulted in anticonvulsant activity. The size of the annelated ring and the character and position of the cycloalkyl ring and its substituents seemed to have a significant influence on the strength of the anticonvulsant activity. The rank order of potency according to the size of the annelated ring was as follows: diazepine > pyrimidine > imidazole. Among investigated diazepinopurinediones most compounds (78%) showed protective

Table 5
Anticonvulsant activity and neurotoxicity of selected compounds after oral administration (30 mg/kg or 50 mg/kg) to rats.

Compound[a]	MES[b]				ScMet[b]					Toxicity[b]				ED_{50} [mg/kg]
	0.5 h	1 h	2 h	4 h	0.25 h	0.5 h	1 h	2 h	4 h	0.25 h	0.5 h	1 h	4 h	
8	–	30 (1/4)	–	–	–	–	–	–	–	–	–	–	–	
17	–	–	–	–	50 (3/4)	50 (2/4)	50 (3/4)	50 (1/4)	50 (2/4)	–	–	–	–	>200 ScMet 0.25 h
20	–	30 (2/4)	30 (1/4)	30 (1/4)	–	–	–	–	–	–	–	–	–	
29	–	–	–	–	50 (1/4)[c]	50 (1/4)[c]	50 (1/4)[c]	–	50 (1/4)[c]	–	–	–	–	
31	–	–	–	–	–	50 (2/4)	–	50 (1/4)	–	–	–	–	–	>250 (MES) >100 (ScMet)[c]
Valproate														287 (MES) 209 (ScMet)

The dash (–) indicates an absence of activity/toxicity at the given dose administration.
[a] Given as a suspension in 0.5% methylcellulose.
[b] Meaning of figures in anticonvulsant test: e.g. 1/4 means the number of animals protected/number of animals tested.
[c] Death following continuous seizures.

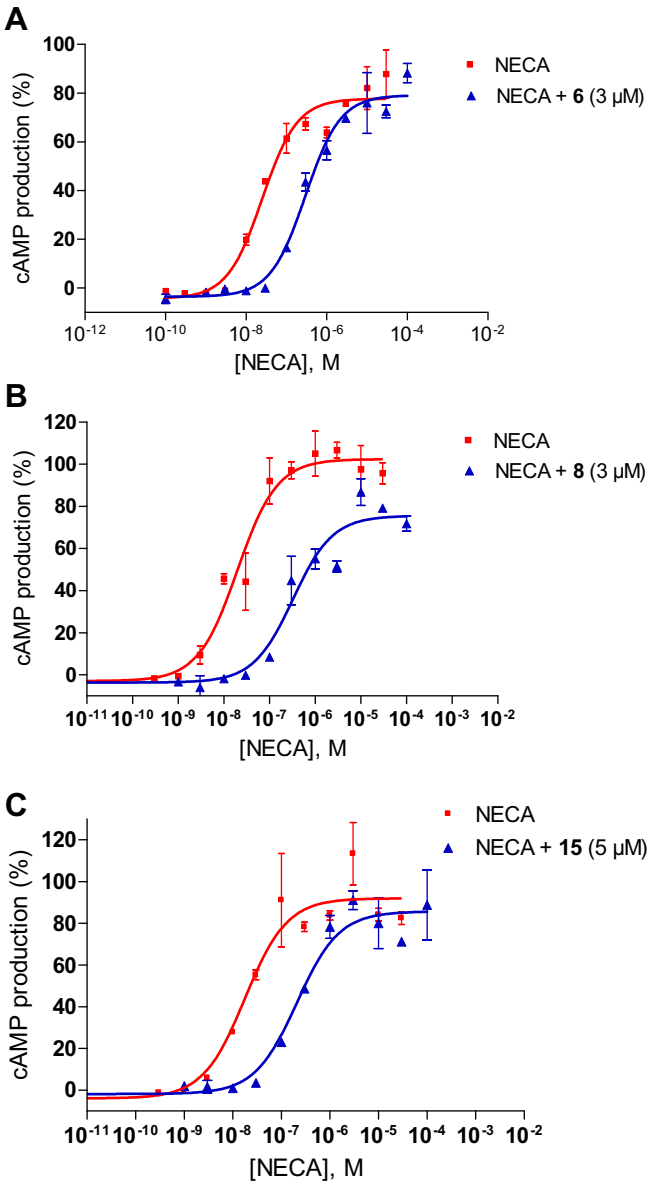

Fig. 8. cAMP accumulation studies in CHO cells expressing the human adenosine A_{2A} receptor by different concentrations of the agonist NECA in the absence and presence of test compound **6** (A), **8** (B) or **15** (C). All three investigated compounds shifted the concentration–response curves for NECA to the right. Apparent K_b values could be calculated as follows: 210 ± 51 nM (**6**), 220 ± 39 nM (**8**), and 644 ± 156 nM (**15**).

activity in the chemical test (compound **31** in both tests at short time, 0.5 h). Introducing a substituent at the cyclohexyl ring resulted in anticonvulsant activity while the unsubstituted cyclohexyl compound **26** was inactive. Among active substances three compounds **27**, **28**, **33** showed neurotoxicity at a dose of 100 mg/kg, which was lower than the effective dose (300 mg/kg). All the other compounds were nontoxic. The two most active derivatives **29** and **31** were also administered orally to rats (Table 5). Compound **31** showed protection in ScMet test at 0.5 h and 2 h time at a dose of 50 mg/kg with no symptoms of neurotoxicity. The ED_{50} determined for compound **31** was >100 mg/kg in the chemical test and >250 mg/kg in the electric test (Table 5). Compound **29** showed protection in the ScMet test at 0.5–4 h time at a dose of 50 mg/kg but caused death following seizures.

Among pyrimidopurinedione derivatives 59% of investigated substances showed anticonvulsant activity in chemical tests or in both tests (compounds **8**, **20**). In this group of compounds introducing substituents to the cyclohexyl ring did not increase anticonvulsant potency in comparison to unsubstituted compound **11**. The majority of substances in this group (except compounds **10**, **11**, **12**, **13**) showed neurotoxicity at 300 mg/kg.

Three compounds: **8**, **17**, **20** were administered orally to rats, showing protection from 1 to 4 h at 30 mg/kg (compounds **8**, **20**) in the electric test or at 50 mg/kg (compound **17**) in the chemical test without symptoms of neurotoxicity. For compound **17** the ED_{50} (>200 mg/kg) was determined. Imidazopurinediones were the least active compounds as anticonvulsants, only 33% of the investigated compounds showed weak anticonvulsant activity in chemical seizures at a high dose of 300 mg/kg with neurotoxicity at the same dose (compounds **1**, **4**) or even at lower dose (compound **3**).

The anticonvulsant activity of the examined compounds was analysed for correlation with AR affinity and some coincidence of adenosine A_{2A} affinity and anticonvulsant activity was observed. The best A_{2A} ligands among pyrimido- and diazepinopurinediones

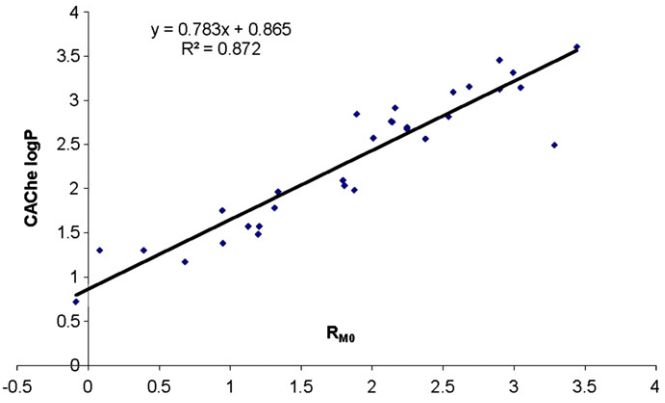

Fig. 9. Correlation between R_{M0} and log *P* values calculated by CAChe 6.1.

showed also the best anticonvulsant activity (compounds **8**, **15**, **17**, **20**, **21**, **29**). This correlation was significantly distinct in compound **20**. *S*-Configuration was beneficial for both activities. Suggestions in recent work [55] of proconvulsant but not anticonvulsant effects of adenosine receptor antagonists were not confirmed in this study and the correlation is not clear. The selectivity profile appears to be important, A_{2A}-selective AR antagonists being neuroprotective while A_1 antagonists may show proconvulsant effects.

5. Physicochemical properties

Parameters of lipophilicity expressed by R_{MO} values were determined using planar RP-TLC. The theoretical partition coefficients (log *P*) were also calculated in Project Leader application incorporated into the CAChe 6.1 software [56] using the atom typing scheme of Ghose and Crippen [57].

The calculated and experimental lipophilicity values of the examined compounds are collected in the Table in Supplementary data. The R_{M0} values are in the range from −0.085 (compound **5**) to 3.442 (compound **33**). For a number of compounds the R_{M0} values are below 2, which may suggest weak BBB permeation. It can be observed that for the analogous compounds, e.g. **1**, **10**, **25** or **2**, **17**, **31**, the R_{M0} values increase with the size of the annelated ring. For structural isomers **15**–**17** as well as **29**–**31** the values of lipophilicity are the same. Interestingly for the mixtures of *cis*/*trans* isomers (compounds **5**, **15**, **16**, **28**, **29**, **30**) values of R_{M0} did not differ and only one spot on the plate could be observed, instead of the expected two spots, for the *cis* and the *trans* form. This differentiation was seen only for two substances **12** and **27**, where two spots for *cis* and *trans*isomers were obtained.

The correlation coefficient R^2 was estimated for experimental and calculated partition coefficients by means of linear regression analysis. The determined R^2 was 0.87 suggesting high correlation of the calculated log *P* with the experimental R_{MO} values (Fig. 9). However, there was no correlation between adenosine receptor affinity of the compounds and their partition coefficients. It can be concluded that the proper range of lipophilicity is clearly not the only parameter relevant for adenosine receptor affinity.

Table 6
A_{2A} AR QSAR model. Summary of the statistics.

Number of compounds	31
r^{2a}	0.77
q^{2b}	0.68
k^c	0.70
k'^c	1.00

[a] Regression coefficient.
[b] Cross-validated regression coefficient.
[c] Slopes of regression lines.

6. QSAR prediction

The process of QSAR model development can be generally divided into three stages: data preparation, data analysis, and model validation. The first stage includes the selection of a molecular dataset, calculation of molecular descriptors, and the choice of the QSAR approach in terms of the statistical methods of data analysis and correlation. The second part involves the building of models that correlate descriptor values with those of biological activity. The final part of QSAR model development is the model validation [58]. In the present study the investigations have been performed for the dataset of 32 active A_{2A} adenosine receptor ligands.

6.1. Model building

The dataset was randomly split into two sets: training set (TS) for model building and prediction set (PS) for the model validation prediction. The TS contained 82% of the tested ligands and the PS 18% covering the whole range of binding affinities [59]. For developing QSAR equations for A_{2A} AR binding affinity prediction the set of 39 ligands TS and PS contained 32 and 7 compounds, respectively.

The structures of the synthesized compounds were built in CAChe 7.6 workspace [60]. The topological, geometric and electronic descriptors [59] were calculated in CAChe 7.6 Project Leader application.

Determination of the equation that best represented the dependence of the A_{2A} AR binding affinity on several input descriptors was carried out using the MLR (multiple linear regression) technique incorporated into the Project Leader CAChe 7.6 application [60] using a randomized training set and a described procedure [32].

All the models having cross-validated $q^2 > 0.50$ and a regression coefficient $r^2 > 0.60$ were collected. Two outliers within the TS, that did not fit the model and which could probably act involving another receptor binding mode, were identified and excluded. The total amount of these outliers was not exceeding 7% of the TS. More that 30 models were collected.

6.2. Model validation

The predictive ability of a QSAR model can only be estimated using an external test set of compounds (PS) that was not used for building the model. The following criteria for a QSAR model to have high predictive power should be satisfied [58,61]:

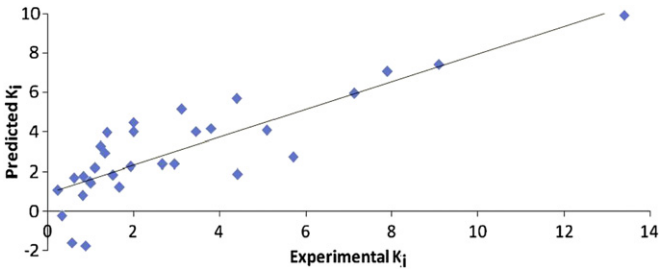

Fig. 10. Experimental vs. predicted K_i values [μM] obtained by using the QSAR equation.

Table 7
Summary of the statistics for the A_{2A}AR QSAR model. Validation protocol.

Number of compounds	6
q^2	0.88
R	0.96
R^2	0.92
k	0.92
k'	0.99

1. high value of cross-validated coefficient after leave-one-out procedure $q^2 > 0.5$, non-cross-validated regression coefficient $r^2 > 0.6$ (Table 6, Fig. 10);
2. correlation coefficient R between the predicted and observed activities of compounds from an external test set (PS) close to 1 (Table 7, Figs. 11 and 12);
3. at least one of the correlation coefficients for regressions through the origin (predicted versus observed activities, or observed versus predicted activities), i.e. R'^2 or R''^2 should be close to R^2 (Table 7, Figs. 11 and 12) or
4. slopes k and k' of regression lines (predicted versus observed activities, or observed versus predicted activities) through the origin $0.85 \leq k \leq 1.15$, $0.85 \leq k' \leq 1.15$ (Table 7, Figs. 11 and 12);

To validate the obtained 3D-QSAR models we selected 6 molecules with a different spectrum of structure and affinity (prediction test PS). The statistics for the best model is shown in Table 6 and Fig. 7. The best 3D-QSAR model obtained is:

$$K_i(A_{2A}\ AR) = -2.546^*\log P - 18.674^*E_{HOMO} + 0.007^*SA_{i-} + 0.049^*S_{ED} - 92.3163, \quad (1)$$

where $\log P$ – octanol/water partition coefficient, E_{HOMO} – HOMO energy, SA_{i-} – surface area of the negative-charged electrostatic isopotential, S_{ED} – surface area of the electrostatic potential on electron density.

The best equation (1) predicted the affinity in the PS with a correlation coefficient between predicted and observed affinity of $R = 0.96$, Table 6, Fig. 11. The predicted K_i values were close to the experimental values, as shown in Fig. 12. For the best model obtained the statistical criteria are as follows (Table 7).

The first descriptor in the A_{2A} AR QSAR model is $\log P$ with a negative contribution coefficient, i.e. the higher the $\log P$ value of the molecule, the better the A_{2A} AR affinity of the ligand. Preferable would be a six- or seven-membered annelated ring with cyclohexyl and larger substituents. The second descriptor in Eq. (1) is E_{HOMO} – the energy required to remove an electron from the highest occupied molecular orbital. In general, this term characterizes the reactivity of the molecule, the ability to form bonds. As E_{HOMO} has a negative value and a negative contribution coefficient, the higher energy HOMO would result in better A_{2A} AR affinity. Here the preference is given to the 6-membered third cycle and large cycloalkyl substituents. The surface area of the negatively charged electrostatic potential (SA_{i-}) represents the distance from the structure at which a proton experiences a set attraction. The value of the electrostatic potential on the surface is ±18 kcal/mol. A positive contribution coefficient implies that this descriptor should have a small SA_{i-} value to possess higher affinity. Indeed, the ligands in this series with polar electronegative substituents are not favourable for A_{2A} AR affinity. The last descriptor in Eq. (1) is the surface area of the electrostatic potential on electron density that represents charge distribution in a molecule and also is a more accurate representation of the true shape of the ligand. Its positive contribution coefficient suggests that this surface area should be small. Taking into account the preferences for the ligand – which is a 6- or 7-membered annelated ring with a bulky cycloalkyl substituent, the last descriptor might suggest that the molecule should also have a twisted conformation in order possess a smaller surface area.

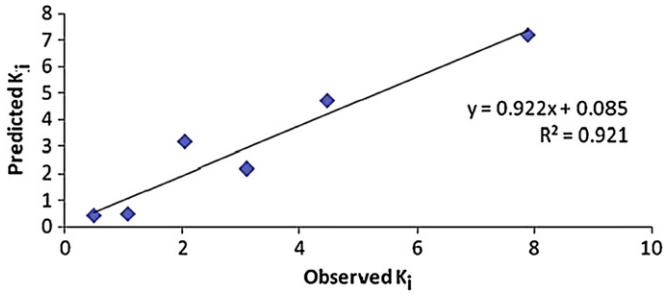

Fig. 11. Experimental vs. predicted K_i values [μM] for the external test set.

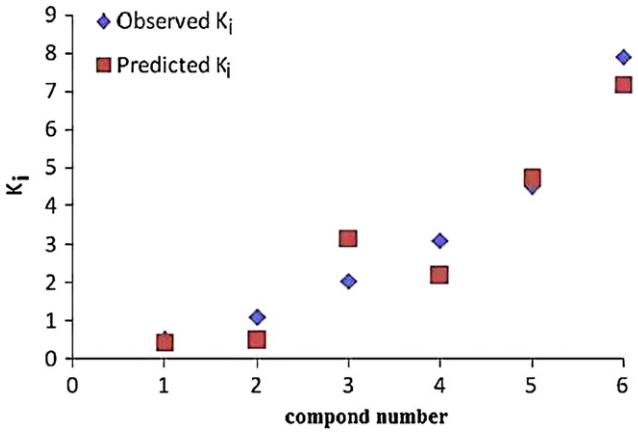

Fig. 12. Comparison of experimental K_i values (■)[μM] with those predicted by the QSAR model (◆).

In conclusion, the obtained 3D-QSAR model (**1**) accurately predicted A_{2A} AR affinity of cycloalkyl-substituted tricyclic xanthine derivatives. Introduction of 3D-properties such as surface areas of the potentials significantly improved the predictive ability of the equation. It appears that the ligand binding affinity strongly depends on the electron surface properties of the molecule. The analysis of the obtained equation outlined the preferences for A_{2A} AR ligands and therefore will be helpful for further design of A_{2A}-selective AR antagonists.

7. Conclusions

A series of 33 new cycloalkyl derivatives of imidazo-, pyrimido- and 1,3-diazepino[2,1-*f*]purinediones were obtained. The new compounds were tested for their adenosine receptor affinity and exhibited selectivity for adenosine A_{2A} receptors. The most potent A_{2A} antagonists were found among the pyrimido[2,1-*f*]purinediones, while 1,3-diazepino[2,1-*f*]purinediones showed the best anticonvulsant properties. Lipophilicity was not correlated with the observed pharmacological activities. It was assumed that small differences in the shape and significant changes in the electrostatic potentials are responsible for the differences in activity. A QSAR model, able to predict the A_{2A}R affinity within the group of tricyclic xanthine derivatives possessing cycloalkyl substituents, was proposed and validated. This approach can be considered useful for further search for tricyclic xanthine antagonists possessing the desired high A_{2A} AR binding affinity. In addition, the cycloalkyl-

substituted tricyclic xanthine derivatives contain a basic nitrogen atom, which can easily be protonated, and thus leads to increased water-solubility in comparison to most other xanthine derivatives as well as non-xanthine AR antagonists.

8. Experimental protocols

8.1. Chemistry

Melting points were determined on a Mel-Temp II apparatus. IR spectra were taken as KBr discs on an FT Jasco IR 410 apparatus. ^{1}H NMR spectra were performed with a Varian Mercury 300 MHz spectrometer in DMSO-d_6 (**5**, **12**, **13**) or $CDCl_3$ (the remaining compounds) with TMS as an internal standard. UV spectra were recorded on a UV–Vis V530 spectrophotometer at a concentration of 1×10^{-5} mol/L in methanol. Elemental analyses (C, H and N) were performed on an Elemental Vario-EL III apparatus and were in accordance with theoretical values within ±0.4%. TLC data were obtained with Merck Silica Gel 60F_{254} aluminum sheets with developing systems A, B, C. Spots were detected under UV light. Measurements of optical rotation were carried out on a Jasco Dipol 1000 polarimeter conc. 2 in ethanol (c = 2 g/100 ml, ethanol). Spectroscopic data are presented in Table 2.

8.1.1. General procedure for the synthesis of cycloalkyl-substituted 1,3-dimethyl-6,7,8,9-tetrahydro-(8H)-imidazopyrimido-6,7,8,9-tetrahydro(10H)-1,3-diazepino[2,1-f]purine-2,4-(1H,3H)-diones (**1**–**33**) (except: **14**, **18**, **28**)

A mixture of 0.73 g (2 mmol) of 7-(2-bromoethyl)-8-bromotheophylline, 0.66 g (2 mmol) of 7-(3-chloropropyl)-8-bromotheophylline, 0.79 g (2 mmol) of 7-(4-bromobutyl)-8-bromoth eophylline and the appropriate amine (2–20 fold excess) was refluxed in DMF, butanol, xylene, or Me-Digol, or without solvent (compounds **5**, **11**, **26**) for 5–10 h (see Table 1). The progress of the cyclization was monitored by thin layer chromatography (TLC). The reaction was carried out until the spot of the starting material had disappeared. After cooling the precipitate was separated (compounds **1**, **2**, **4**, **7**, **10**, **13**, **15**, **17**, **22**, **23**, **24**, **30**) and washed with ethanol and water. Other compounds precipitated by cooling and adding water (**8**, **9**, **12**, **16**, **19**, **20**, **21**, **25**, **26**, **27**, **31**, **32**, **33**) to the reaction mixture. Some compounds were separated after distillation of solvent and adding water (**5**, **29**) or water and NaOH (**6**). Acetyl derivatives **14**, **28** were prepared by refluxing compounds **13** and **27** with acetic anhydride for 5 h, removing the excess of anhydride by distillation under reduced pressure and crystallization of the residue.

Optically active compounds **19**, **20** were obtained by cyclization of 7-(3-chloropropyl)-8-bromotheophylline with commercially available enantiomerically pure *S*(+)-1-cyclohexylethylamine ($[\alpha]_D^{20} = +3.8 \pm 0.3$ (Fluka)) and *R*(−)-1-cyclohexylethylamine ($[\alpha]_D^{20} = -3.8 \pm 0.3$ (Fluka)). Racemic compound **18** was a stoichiometric mixture of compounds **19** and **20**. Spectroscopic data are presented in Table 8. The elemental analyses can be found in Supplementary data.

8.2. X-ray structure analysis

Crystal data for **7**: $C_{13}H_{17}N_5O_2$, $M = 275.32$, monoclinic, space group $P2_1/c$, $a = 8.3797(9)$ Å, $b = 16.6762(16)$ Å, $c = 9.6895(8)$ Å, $\beta = 105.482(10)^\circ$, $V = 1304.9(2)$ Å^3, $Z = 4$, $D_x = 1.401$ g cm^{-3}, $T = 293$ K, $\mu = 0.099$ mm^{-1}, $\lambda = 0.71073$ Å, data/parameters = 2286/185; final $R_1 = 0.0460$.

Crystal data for **13**: $C_{16}H_{23}N_5O_3 \cdot CH_3OH$, $M = 365.44$, monoclinic, space group $P2_1/c$, $a = 9.7248(2)$ Å, $b = 36.4797(7)$ Å, $c = 5.1337(1)$ Å, $\beta = 92.671(1)^\circ$, $V = 1819.24(6)$ Å^3, $Z = 4$, $D_x = 1.334$ g cm^{-3}, $T = 293$ K, $\mu = 0.12$ mm^{-1}, $\lambda = 1.54178$, data/parameters = 3368/252; final $R_1 = 0.0527$.

Crystal data for **33**: $C_{19}H_{29}N_5O_2$, $M = 359.47$, orthorhombic, space group $Pna2_1$, $a = 23.9625(14)$ Å, $b = 11.4933(6)$ Å, $c = 20.9751(16)$ Å, $V = 5776.7(6)$ Å^3, $Z = 12$, $D_x = 1.240$ g cm^{-3}, $T = 293$ K, $\mu = 0.083$ mm^{-1}, $\lambda = 0.71073$ Å, data/parameters = 9093/839; final $R_1 = 0.0540$.

The crystals of **7**, **13** and **33** were obtained by slow evaporation from methanol and propanol (1:1) solutions. The measurements of **7** and **33** crystals were performed on a Kuma4CCD κ-axis diffractometer with graphite-monochromated Mo Kα radiation ($\lambda = 0.71073$ Å) at room temperature. While for **13** measurements were performed on a SMART diffractometer with graphite-monochromated Cu Kα radiation ($\lambda = 1.154178$ Å) at room temperature. The structures were solved by direct method using the SHELXTS program [62]and refined with SHELXTL [63]. E-map provided positions for all non-H-atoms. The full-matrix least-squares refinement was carried out on F^2 using anisotropic temperature factors for all non-H-atoms in **7** and **33**. While in **13** mobile solvent atoms, located in the channel down *c*-axis, were left with isotropic temperature factors. In structures **13** and **33** positional disorder for carbon atoms was identified and refined. In structure **13**, the H-atoms attached to O17 and O1s were located in difference Fourier map and their positions were refined freely with $U_{iso} = 1.5U_{eq}$(O). For all three structures H-atoms bonded to carbons were placed in idealized position and considered to ride on their parent atoms.

Special comments to structure **33**: The structure was solved and refined in $Pna2_1$ non-centrosymmetric space group with three molecules in independent crystallographic unit. Two of them differ insignificantly in cyclooctyl conformation. The third one, with disordered diazepine and cyclooctyl (both with s.o.f. = 0.5), consists in fact two identical molecules repeat by mirror. The final R_1-factor equals 0.0540. After transformation to *Pnma* centrosymmetric space group with one molecule in general and the other in special position, final R_1 stopped at 0.12. Therefore refinement of the structure **33** was left in a non-centrosymmetric space group.

Crystallographic data (excluding structural factors) for the structure reported in this paper have been deposited with the Cambridge Crystallographic Data Centre and allocated the deposition numbers: (CCDC 741160–741162) for compounds **7**, **13** and **33** respectively. Copies of the data can be obtained free of charge on application to CCDC, 12 Union Road, Cambridge CB2 1EW, UK (fax: +44 1223 336 033; e-mail: deposit@ccdc.cam.ac.uk).

8.3. Pharmacology

8.3.1. Adenosine receptor binding assays

Adenosine binding assays were performed as previously described [49,64] using rat brain cortical membrane preparations for A_1 AR assays and rat brain striatial membrane preparations for A_{2A} assays. Frozen rat brains (unstripped) were obtained from Pel-Freez®, Rogers, Arkansas, USA. For assays at human A_1, A_{2A}, A_{2B} and A_3, ARs, CHO cell membranes expressing the human receptors were used as described [65]. [^{3}H]2-chloro-N^6-cyclopentyladenosine ([^{3}H]CCPA) was used as the A_1 radioligand, [^{3}H]3-(3-hydroxypropyl)-7-methyl-8-(*m*-methoxystyryl)-1-propargylxanthine ([^{3}H]MSX-2) as the A_{2A} radioligand, [^{3}H]4-(2-[7-amino-2-(2-furyl)-[1,2,4]-triazolo-[2,3-*a*]-[1,3,5]-triazin-5ylamino]ethyl)phenol ([^{3}H]ZM241385) and [^{3}H]8-(4-(4-(4-chlorophenyl)piperazine-1-sulfonyl)phenyl)-1-propylxanthine ([^{3}H]PSB-603) as A_{2B} receptor radioligands and [^{3}H]phenyl-8-ethyl-4-methyl-(8*R*)-4,5,7,8-tetrahydro-1*H*-imidazo[2,1-*i*]purine-5-one ([^{3}H]PSB-11) as the A_3 AR radioligand. Initially, a single high concentration of compound (25 μM at A_1 and A_{2A}, 10 μM at A_{2B} and A_3 receptors) was tested in three (A_1, A_{2A}) or two (A_{2B}, A_3) independent

Table 8
Spectral data of cycloalkylpyrimido-, imidazo- and diazepino[2,1-*f*]purinediones.

Compound	UV λ_{max}	IR ν (cm^{-1})	^1H NMR δ (ppm)
1	300	1693 − CO (pos. 2) 1648 − CO (pos. 4)	1.64–1.99 (2 m, 8H) cyclopentyl; 3.36 (s, 3H, N_3CH_3); 3.51 (s, 3H, N_1CH_3); 3.84 (t, 2H, $J = 8.10$ Hz, N_5CH_2); 4.05–4.20 (m, 3H, $CH_2N_2 + N_9CH$); 0.98–1.77 (3 m, 11H, cyclohexyl); 3.16 (d, 2H, $J = 7.15$ Hz, N_8CH_2); 3.36 (s, 3H, N_3CH_3); 3.50 (s, 3H, N_1CH_3); 3.86 (q, 2H, $J = 7.43$ Hz, CH_2N_8); 4.19 (q, 2H, $J = 7.29$ Hz, N_5CH_2)
2	302	1700 − CO (pos. 2) 1655 − CO (pos. 4)	0.98–1.77 (3 m, 11H, cyclohexyl); 3.16 (d, 2H, $J = 7.15$ Hz, N_8CH_2); 3.50 (s, 3H, N_1CH_3); 3.86 (q, 2H, $J = 7.43$ Hz, CH_2N_8); 4.19 (q, 2H, $J = 7.29$ Hz, N_5CH_2)
3	[35]		
4	303	1700 − CO (pos. 2) 1651 − CO (pos. 4)	1.49 (2 m, 8H, cyclohexenyl); 2.26 (t, 2H, $J = 7.18$ Hz, CH_2CH_2); 3.36 (s, 3H, N_3CH_3); 3.43 (t, 2H, $J = 7.31$ Hz, N_8CH_2); 3.50 (s, 3H, N_1CH_3); 3.87 (q, 2H, $J = 7.31$ Hz, CH_2N_8); 4.15–4.20 (m, 2H, N_5CH_2); 5.47 (s, 1H, cyclohexenyl)
5	302	3391 − OH 1700 − CO (pos. 2) 1654 − CO (pos. 4)	1.17–1.98 (3, m, 8H, cyclohexyl; 3.13 (s, 3H, N_3CH_3); 3.22–3.26 (m, 2H, CH_2N_9); 3.32 (s, 4H, $N_1CH_3 + 4'$-CH cyclohexyl); 3.98–4.1 (m, 3H, $N_5CH_2 + N_8CH$); 4.57 (d, 1H, $J = 5.00$ Hz, OH)
6	302	1693 − CO (pos. 2) 1648 − CO (pos. 4)	1.59–1.85 (m, 14H, cyclooctyl; 3.37 (s, 3H, N_3CH_3); 3.52 (s, 3H, N_1CH_3); 3.82–3.90 (33H, $CH_2N_8 + N_8CH$); 4.14 (q, 2H, $J = 7.2$ Hz, N_5CH_2)
7	299	1702 − CO (pos. 2) 1653 − CO (pos. 4)	0.72–0.88 (2, m, 4H, cyclopropyl); 2.08–2.16 (m, 2H, $CH_2{-}CH_2{-}CH_2$); 2.65–2.72 (m, 1H, N_9CH); 3.35–3.39 (m, 5H, $N_3CH_3 + CH_2N_9$); 3.54 (s, 3H, N_1CH_3); 4.19 (t, 2H, $J = 6.16$ Hz, N_5CH_2)
8	301.5	1697 − CO (pos. 2)	0.28 (d, 2H, $J = 4.87$ Hz, cyclopropyl; 0.55 (d, 2H, $J = 7.4$ Hz, 2H, cyclopropyl); 1.05–1.038 (m, 1H, cyclopropyl); 2.13–2.20 (m, 2H, $CH_2{-}CH_2{-}CH_2$); 3.36 (s, 3H, N_3CH_3); 3.40–3.48 (m, 4H, $CH_2N_9 + N_9CH_2$); 3.49 (s, 3H, N_1CH_3); 4.22 (t, 2H, $J = 5.90$ Hz, N_5CH_2)
9	302	1699 − CO (pos. 2) 1639 − CO (pos. 4)	1.64–1.75 (m, 2H, $CH_2{-}CH_2{-}CH_2$); 2.09–2.25 (m, 6H, cyclobutyl); 3.35–3.40 (m, 5H, $N_3CH_3 + CH_2N_9$); 3.50 (s, 3H, N_1CH_3); 4.19 (2H, $J = 6.03$ Hz, N_5CH_2); 4.77–4.89 (q, 1H, N_9CH)
10	301.5	1697 − CO (pos. 2) 1664 − CO (pos. 4)	1.56–1.93 (m, 8H, cyclopentyl); 2.05–2.13 (m, 2H, $CH_2{-}CH_2{-}CH_2$); 3.28 (t, 2H, $J = 5.63$ Hz, CH_2N_9); 3.34 (s, 3H, N_3CH_3); 3.48 (s, 3H, N_1CH_3); 4.18 (t, 2H, $J = 6.04$ Hz, N_5CH_2); 4.73–4.83 (m, 1H, N_9CH)
11	[35]		
12	301	3484 − OH 1701 − CO (pos. 2) 1652 − CO (pos. 4)	1.21–2.01 (m, 10H, cyclohexyl + $CH_2{-}CH_2{-}CH_2$); 3.13 (s, 3H, N_3CH_3); 3.23–3.37 (m, 5H, $N_1CH_3 + CH_2N_9$); 3.80 (s, 1H, 4-cyclohexyl); 3.98–4.1 (m, 3H, $N_5CH_2 + N_9CH$); 4.38 (s, 1H, OH ax); 4.56 (s, 1H, OH eq)
13	302	3384 − OH 1702 − CO (pos. 2) 1660 − CO (pos. 4)	1.16–1.30 (m, 2H, cyclohexyl); 1.58–1.68 (m, 4H, cyclohexyl); 1.85–1.98 (2m, 2H, $CH_2{-}CH_2{-}CH_2$ + cyclohexyl); 3.11 (s. 3H, N_3CH_3); 3.24 (t, 2H, $J = 6.33$ Hz, CH_2N_9); 3.30 (s, 3H, N_1CH_3); 3.40–3.49 (m, 1H, 4′-cyclohexyl); 3.97–4.11 (m, 3H, $N_5CH_2 + N_9CH$); 4.56 (t, 1H, $J = 4.38$ Hz. OH)
14	301	1731 − ($OCOCH_3$) 1698 − CO (pos. 2) 1650 − CO (pos. 4)	1.51–1.73 (m, 4H, cyclohexyl); 1.81–1.85 (m, 2H, $CH_2CH_2CH_2$); 2.04–2.14 (m, 7H, $OCOCH_3$ + cyclohexyl); 3.27 (t, 2H, $J = 5.52$ Hz, CH_2N_9); 3.36 (s, 3H, N_3CH_3); 3.51 (s, 3H, N_1CH_3); 4.17–4.29 (m, 3H, $N_5CH_2 + 4'$-CH cyclohexyl); 4.63–4.70 (m, 1H, N_9CH)
15	304	1720 − CO (pos. 2) 1655 − CO (pos. 4)	0.921–1.03 (d, 3H, $J = 6.25$ Hz. $J = 7.00$ Hz, *cis*/*trans* CH_3); 1.51–1.98 (m, 9H, cyclohexyl); 2.06–2.15 (m, 2H, $CH_2{-}CH_2{-}CH_2$); 3.08–3.36 (m, 5H, $N_3CH_3 + CH_2N_9$); 3.50 (s, 3H, N_1CH_3); 4.17–4.22 (m, 3H, N_5CH_2, N_9CH)
16	303	1698 − CO (pos. 2) 1655 − CO (pos. 4)	0.86 (d, 2H, $J = 6.41$ Hz, CH_3); 0.95 (d, 1H, $J = 7.18$ Hz, CH_3); 1.14–1.87 (m, 9H, cyclohexyl); 2.05–2.13 (m, 2H, $CH_2{-}\mathbf{CH_2}{-}CH_2$); 3.24–3.34 (m, 2H, CH_2N_9); 3.36 (s. 3H, N_3CH_3); 3.50 (s, 3H, N_1CH_3); 4.07–4.31 (m, 3H, N_5CH_2, N_9CH)
17	303.5	1705 − CO (pos. 2) 1651 − CO (pos. 4)	0.97–1.27 (m, 10H, cyclohexyl); 1.66–1.76 (m, 2H, $CH_2{-}CH_2{-}CH_2$); 3.35 (d. 7H, $J = 5.77$ Hz, $N_3CH_3 + CH_2N_9 + N_9CH_2$); 3.50 (s, 3H, N_1CH_3); 4.21 (t, 2H, $J = 6.04$ Hz, N_5CH_2)
18	303	1699 − CO (pos. 2) 1656 − CO (pos. 4)	0.94–1.80 (m, 14H, cyclohexyl + CH_3); 2.06–2.15 (m, 2H, $CH_2{-}CH_2{-}CH_2$); 3.18–3.31 (m, 2H, CH_2N_9); 3.36 (s, 3H, N_3CH_3); 3.50 (s, 3H, N_1CH_3); 4.11–4.26 (m, 3H, $N_5CH_2 + N_9CH$)
19[a]	303	1699 − CO (pos. 2) 1656 − CO (pos. 4)	0.95–1.79 (m, 14H, cyclohexyl + CH_3); 2.07–2.14 (m, 2H, $CH_2{-}CH_2{-}CH_2$); 3.16–3.30 (m, 2H, CH_2N_9); 3.36 (s, 3H, N_3CH_3); 3.49 (s, 3H, N_1CH_3); 4.11–4.27 (m, 3H, $N_5CH_2 + N_9CH$)
20[b]	303	1699 − CO (pos. 2) 1656 − CO (pos. 4)	0.95–1.80 (m, 14H, cyclohexyl + CH_3); 2.07–2.14 (m, 2H, $CH_2{-}CH_2{-}CH_2$); 3.16–3.31 (m, 2H, CH_2N_9); 3.36 (s, 3H, N_3CH_3); 3.49 (s, 3H, N_1CH_3); 4.11–4.27 (m, 3H, N_5CH_2); 4.49 (t, 1H, $J = 7.06$ Hz, N_9CH)
21	303	1698 − CO (pos. 2) 1658 − CO (pos. 4)	1.46–1.62 (m, 4H, cyclohexenyl); 1.92–2.01 (m, 4H, cyclohexenyl); 2.14–2.17 (2H, $CH_2{-}CH_2{-}CH_2$); 2.25 (t, 2H, $J = 6.92$ Hz, $CH_3\mathbf{C}H_2$); 3.28–3.47 (m, 5H, $N_3CH_3 + CH_2N_9$); 3.50 (s, 3H, N_1CH_3); 3.60 (t, 2H, $J = 7.18$ Hz, N_9CH_2); 4.19 (t, 2H, $J = 6.08$ Hz, N_5CH_2); 5.13 (s, 1H, cyclohexenyl)
22	303	1698 − CO (pos. 2) 1652 − CO (pos. 4)	1.51–1.87 (m, 12H, cycloheptyl); 2.04–2.11 (m, 2H, $CH_2{-}CH_2{-}CH_2$); 3.30 (t, 2H, $J = 5.62$ Hz, CH_2N_9); 3.35 (s, 3H, N_3CH_3); 3.51 (s, 3H, N_1CH_3); 4.17 (t, 2H, $J = 6.04$ Hz, N_5CH_2); 4.34–4.40 (m, 1H, N_9CH)
23	303.5	1702 − CO (pos. 2) 1653 − CO (pos. 4)	1.55–1.83 (m, 14H, cyclooctyl); 2.04–2.12 (m, 2H, $CH_2CH_2CH_2$); 3.31 (t, 2H, $J = 5.63$ Hz, CH_2N_9); 3.36 (s, 3H, N_3CH_3); 3.51 (s, 3H, N_1CH_3); 4.18 (t, 2H, $J = 6.04$ Hz, N_5CH_2); 4.48–4.52 (m, 1H, N_9CH)
24	304	1700 − CO (pos. 2) 1655 − CO (pos. 4)	1.71 (s, 6H, adamantyl); 2.04–2.09 (m, 2H, $CH_2CH_2CH_2$); 2.16–2.27 (m, 9H, adamantyl); 3.36 (s, 3H, N_3CH_3); 3.43 (t, 2H, $J = 5.64$ Hz, CH_2N_9); 3.51 (s, 3H, N_1CH_3); 4.16 (t, 2H, $J = 6.16$ Hz, N_5CH_2)
25	301	1699 − CO (pos. 2) 1644 − CO (pos. 4)	1.46–2.05 (3m, 12H, cyclopentyl + $CH_2CH_2CH_2CH_2$); 3.12 (t, 2H, $J = 5.13$ Hz, CH_2N_{10}); 3.37 (s, 3H, N_3CH_3); 3.52 (s, 3H, N_1CH_3); 4.30 (t, 2H, $J = 5.26$ Hz, N_5CH_2); 4.38–4.64 (m, 1H, $N_{10}CH$)
26	302.5	1698 − CO (pos. 2) 1656 − CO (pos. 4)	1.32–1.51 (m, 10H, cyclohexyl); 1.80–2.00 (m, 4H, $CH_2CH_2CH_2CH_2$); 3.20 (t, 2H, $J = 4.72$ Hz, CH_2N_{10}); 3.37 (s, 3H, N_3CH_3); 3.51 (s, 3H, N_1CH_3); 3.89–3.91 (m, 1H, $N_{10}CH$); 4.26–4.30 (m, 2H, N_5CH_2)
27	301	3442 − OH 1696 − CO (pos. 2) 1657 − CO (pos. 4)	1.43–1.94 (m, 12H, cyclohexyl + $CH_2CH_2CH_2CH_2$); 2.06 (d, 1H, $J = 11.8$ Hz, 4′-cyclohexyl); 3.14–3.23 (dt, 2H, $J = 5.52$ Hz, $J = 5.39$ Hz, CH_2N_{10}); 3.36 (s, 3H, N_3CH_3); 3.50 (s, 3H, N_1CH_3); 3.51–3.62 (m, 1H, OH); 3.87–3.98 (m, 1H, $N_{10}CH$); 4.08 (s, 1H, OH *trans*); 4.28 (t, 2H, $J = 4.8$ Hz, N_5CH_2)
28	300	1731 − $OCOCH_3$ 1698 − CO (pos. 2) 1669 − CO (pos. 4)	1.51–1.69 (m, 10H, cyclohexyl); 1.70–2.00 (m, 7H, cyclohexyl + $OCOCH_3$); 2.04–2.11 (m, 4H, $CH_2CH_2CH_2CH_2$); 3.13–3.22 (m, 2H, CH_2N_{10}); 3.37 (s, 3H, N_3CH_3); 3.51 (s, 3H, N_1CH_3); 3.91–3.96 (m, 1H, $N_{10}CH$); 4.27–4.32 (m, 2H, N_5CH_2)
29	301	1699 − CO (pos. 2) 1656 − CO (pos. 4)	0.91–1.02 (dd, 3H, $J = 6.41$ Hz, $J = 7.18$ Hz, *cis*/*trans* CH_3); 1.01–1.18 (m, 1H ax, 4′-cyclohexyl); 1.33–1.48 (1H eq, 4′-cyclohexyl); 1.67–1.91 (m, 12H, cyclohexyl + $CH_2{-}CH_2{-}CH_2{-}CH_2$); 3.16–3.23 (m, 2H, CH_2N_{10}); 3.37 (s. 3H, N_3CH_3); 3.51 (s, 3H, N_1CH_3); 3.79–3.92 (m, 1H, $N_{10}CH$); 4.26–4.30 (m, 2H, N_5CH_2)
30	303	1698 − CO (pos. 2) 1656 − CO (pos. 4)	0.92–1.01 (dd, 3H, $J = 7.8$ Hz, $J = 6.41$ Hz, *cis*/*trans* CH_3); 1,1–2.01 (m, 12H, cyclohexyl + $CH_2{-}\mathbf{CH_2}{-}CH_2$); 3.02–3.35 (m, 2H, CH_2N_{10}); 3.36 (s, 3H, N_3CH_3); 3.51 (s, 3H, N_1CH_3); 3.60–3.64 (m, 1H, $N_{10}CH$); 3.99–4.01 (m, 1H, 2cyclohexyl ax); 4.1–4.13 (m, 1H, 2′-cyclohexyl eq); 4.29–4.65 (2m, 2H, N_5CH_2)
31	300	1698 − CO (pos. 2) 1663 − CO (pos. 4)	0.88–1.72 (3m, 11H, cyclohexyl); 1.75–1.95 (m, 4H, $CH_2{-}CH_2CH_2{-}CH_2$); 3.25 (t, 2H, $J = 5.13$ Hz, CH_2N_{10}); 3.37 (s, 5H, $N_3CH_3 + N_{10}CH_2$); 3.51 (s, 3H, N_1CH_3); 4.32 (t, 2H, $J = 5.13$ Hz, N_5CH_2)

(*continued on next page*)

Table 8 (*continued*)

Compound	UV λ_{max}	IR ν (cm^{-1})	^1H NMR δ (ppm)
32	302	1695 − CO (pos. 2) 1651 − CO (pos. 4)	1.48–1.63 (m, 4H, cyclohexenyl); 1.86–1.97 (m, 8H, cyclohexenyl + $CH_2CH_2CH_2CH_2$); 2,26 (t, 2H, $J = 7.30$ Hz, $CHCH_2$); 3.23–3.36 (m, 2H, CH_2N_{10}); 3.37 (s, 3H, N_3CH_3); 3.52 (s, 3H, N_1CH_3); 3.52–3.60 (m, 2H, $N_{10}CH_2$); 4.28 (t, 2H, $J = 5.00$ Hz, N_5CH_2), 5.44 (s, 1H, 2′-cyclohexenyl)
33	302	1696 − CO (pos. 2) 1655 − CO (pos. 4)	1.51–1.88 (m, 18H, cyclooctyl + $CH_2CHCH_2CH_2$); 3.13 (t, 2H, $J = 5.13$ Hz, CH_2N_{10}); 3.37 (s, 3H, N_3CH_3); 3.51 (s, 3H, N_1CH_3); 4.16–4.27 (m, 3H, $N_5CH_2 + N_{10}CH$)

[a] $[\alpha]_D^{20} = +33.26$ ($c = 2$ g/100 ml, ethanol) (conc. 2 in ethanol).
[b] $[\alpha]_D^{20} = -33.29$ ($c = 2$ g/100 ml, ethanol) (conc. 2 in ethanol).

experiments. For potent compounds, curves were determined using 6–7 different concentrations of test compounds spanning 3 orders of magnitude. Data were analysed using the PRISM program version 3.0 or 4.0 (Graph Pad, San Diego, CA, USA).

8.3.1.1. Functional assays. Stably transfected CHO cells expressing the human A_{2A} receptor were grown in DMEM-F12 medium (Invitrogen) with 10% fetal calf serum, 100 U/ml penicillin G, 100 μg/ml streptomycin and 1% ultraglutamine at 37 °C and 5% CO_2. For the experiment they were transferred to 24-well plates at a density of 200,000 cells per well. After 24 h the medium was removed and the cells were washed with 500 μl of 37 °C warm Hank's Balanced Salt Solution (HBSS; 20 mM HEPES, 13 mM NaCl, 5.5 mM glucose, 5.4 mM KCl, 4.2 mM $NaHCO_3$, 1.25 mM $CaCl_2$, 1 mM $MgCl_2$, 0.8 mM $MgSO_4$, 0.44 mM KH_2PO_4 and 0.34 mM Na_2HPO_4, pH adjusted to 7.3) containing 1 U/ml of adenosine deaminase (ADA, Sigma). The cells were then incubated in 300 μl of HBSS with ADA at 37 °C and 5% CO_2 for 2 h. Then, 100 μl of the phosphodiesterase inhibitor Ro20-1724 (Hoffmann La Roche; final concentration 40 μM) was added to each well and the cells were incubated for 15 min at 37 °C and 5% CO_2. Then 100 μl of various dilutions of the agonist 5′-N-ethylcarboxamidoadenosine (NECA; Sigma) in the presence or absence of a single concentration of test compound in HBSS containing 5% DMSO were added in triplicates. After 15 min of incubation at 37 °C and 5% CO_2 the supernatant was removed and 500 μl of 90 °C hot lysis buffer consisting of 4 mM EDTA and 0.01% Triton X-100 with the pH adjusted to 7.3 were added. After 1 h of mixing on ice, cAMP amounts of the lysates were determined by competitive radioligand binding experiments [66]. cAMP competition experiments were performed in a final volume of 120 μl containing 50 μl of cell lysates, 30 μl of [^{3}H]cAMP radioligand solution in lysis buffer (final concentration 3 nM) and 40 μl of cAMP binding protein [66] diluted in the same buffer (50 μg per sample). For determining cAMP concentrations 50 μl of various cAMP concentrations were measured instead of cell lysates, to obtain a standard curve. Total binding was determined by adding radioligand and binding protein to lysis buffer, and the background was determined without addition of binding protein. The mixture was incubated for 60 min on ice and filtered through a GF/B glass fiber filter using a cell harvester (Brandel). The filters were washed three times with 2–3 ml of ice-cold 50 mM Tris–HCl buffer, pH 7.4 and subsequently transferred into scintillation vials. The liquid scintillation counting of the filters started after 9 h of incubation in 2.5 ml of scintillation cocktail (Lumag AG, Basel). Three separate experiments were performed. The amount of cAMP was determined by comparison to a standard curve generated for each experiment.

8.3.2. Anticonvulsant screening

The anticonvulsant evaluation was carried out using reported procedures [52,53]. Male albino mice (F-1 strain, 18–25 g) were used as experimental animals. For testing compounds **8**, **17**, **20**, **29**, **31** male albino rats (Sprague-Dawley 100–150 g) were used. Groups of 1–5 mice were used in MES, ScMet tests, groups of 2–8 animals in the rotorod test. For the evaluation of activity after oral administration, groups of 4 rats were used. The test compounds were suspended in a 0.5% methylcellulose/water mixture. In the preliminary screening each compound was administered as an ip injection at three dose levels (30, 100 and 300 mg/kg) with anticonvulsant activity and neurotoxicity assessed at 0.5 and 4 h intervals after administration. For some compounds also intervals 0.25, 1 and 2 h were applied. Anticonvulsant efficacy was measured by maximal electroshock (MES) and subcutaneous pentylenetetrazole (ScMet), neurological deficit was investigated in the rotorod test; the data are presented in Table 4. Compounds **8**, **17**, **20**, **29**, **31** were examined for oral activity in the rat ScMet and neurotoxicity screen at 30 mg/kg doses (Table 5).

The pharmacological parameters estimated in the preliminary screening were quantified for compounds **17** and **31**. Anticonvulsant activity was expressed in terms of the median effective dose (ED_{50}) in rats after oral administration. For determination of the ED_{50} value groups of 8 rats were given a range of p.o. doses of the test drug until at least three points were established in the range of 10–90% seizure protection. From the plot of this data, the respective ED_{50} values, 95% confidence intervals, slope of the regression line, and the standard error of the slope were calculated by means of a computer program written at NINDS, NIH.

8.4. Determination of lipophilicity

8.4.1. Chromatographic determination of lipophilicity

Methanolic solutions of all compounds were prepared at 1 mg/ml concentration. The solutions were spotted onto TLC plates (20 × 10 cm) precoated with RP-18 silica gel F_{254} (MERCK) using a Hamilton syringe in an amount of 10 μl. A mixture of acetone with water in the range of 50–85% (v/v) in 5% increments was used as a mobile phase. The plates were evaluated in horizontal chromatographic chambers (CHROMODES), saturated with eluent for 45 min (+15 min with plates). The R_M values were calculated from R_f values using the equation: $R_M = \log(1/R_f - 1)$. R_M values were then extrapolated to zero acetone concentration (pure water) by use of equation: $R_M = R_{MO} + bc$.

8.4.2. Calculated lipophilicity

The structures of the ligands were built in CAChe 6.1 [56], the geometry was optimized in MOPAC with PM5 parameters. The lipophilicity was calculated using the CAChe 6.1 Project Leader application with the atom typing scheme of Ghose and Crippen [57].

8.5. QSAR

The structures of the synthesized compounds were built in CAChe 7.6 workspace [60] and the geometry was optimized in MOPAC (Molecular Orbital Package) using semi-empirical Hamiltonian (PM5) to minimize the energy. To find the low-energy conformers the CONFLEX application was used. The energy of each conformation was plotted in a three-dimensional graph. The low-energy conformations, separated by high energy barriers, were collected and optimized using DFT methods B88-LYP functional

with 6-31G** basis set. The topological, geometric and electronic descriptors [59] were calculated in CAChe 7.6 Project Leader application by the atom typing scheme; by Mechanics using Augmented MM3; by MOPAC with PM5 parameters; by DFT methods: D-VWN LDA functional with DZVP basis set or B88-LYP GGA functional with 6-31G** basis set. The statistical parameters were calculated using Project Leader application (for R^2 and q^2) of CAChe 7.6 and Microsoft Excel (for k and k').

Acknowledgements

The authors are grateful to Professor James Stables for providing the biological data through the Antiepileptic Drug Development (ADD) Program of the National Institute of Neurological and Communicative Disorders and Stroke at the National Institute of Health, Bethesda, MD, USA. We thank Dr. Britta Schumacher for performing some of the radioligand binding experiments. This work was partly supported by the Polish Ministry of Science and Higher Education – grants No 2 P05F 022 26 and N N405 297 836 and by the Deutsche Forschungsgemeinschaft (GRK 677).

Appendix. Supplementary data

Supplementary data associated with this article can be found in the online version, at doi:10.1016/j.ejmech.2011.05.023.

References

[1] B.B. Fredholm, A.P. IJzerman, K.A. Jacobson, K.N. Klotz, J. Linden, Pharmacol. Rev. 53 (2001) 527–552.
[2] S. Hess, Exp. Opin. Ther. Pat. 11 (2001) 1533–1561.
[3] L. Yu, H.-Y. Shen, J.E. Coelho, I.M. Araújo, Q.-Y. Huang, Y.-J. Day, N. Rebola, P.M. Canas, E.K. Rapp, J. Ferrara, D. Taylor, C.E. Müller, J. Linden, R.A. Cunha, J.-F. Chen, Ann. Neurol. 63 (2008) 338–346.
[4] D. Elmenhorst, P.T. Meyer, O.H. Winz, A. Matusch, J. Ermert, H.H. Coenen, R. Basheer, H.L. Haas, K. Zilles, A. Bauer, J. Neurosci. 27 (2007) 2410–2415.
[5] A. Bilkei-Gorzo, O.M. Abo-Salem, A.M. Hayallah, K. Michel, C.E. Müller, A. Zimmer, Naunyn-Schmiedeberg's Arch. Pharmacol. 377 (2008) 65–76.
[6] O.M. Abo-Salem, A.M. Hayallah, A. Bilkei-Gorzo, B. Filipek, A. Zimmer, C.E. Müller, J. Pharmacol. Exp. Ther. 308 (2004) 358–366.
[7] B. Schumacher, S. Scholle, J. Hölzl, N. Khudeir, S. Hess, C.E. Müller, J. Nat. Prod. 65 (2002) 1479–1485.
[8] V. Ralevic, G. Burnstock, Pharmacol. Rev. 50 (1998) 413–492.
[9] S.-A. Poulsen, R.J. Quinn, Bioorg. Med. Chem. 6 (1998) 619–641.
[10] J.-L. Moreau, G. Huber, Brain Res. Rev. 31 (1999) 65–82.
[11] C.E. Müller, Drugs Future 25 (2000) 1043–1052.
[12] E. Ongini, P. Schubert, Drug Dev. Res. 45 (1998) 387–393.
[13] F. Impagnatiello, E. Bastia, E. Ongini, A. Monopoli, Emerg. Ther. Targets 4 (2000) 635–663.
[14] J.A. Ribeiro, A.M. Sebastião, A. de Mendonça, Prog. Neurobiol. 68 (2003) 377–392.
[15] J.D. Salamone, A.J. Betz, K. Ishiwari, J. Felsted, L. Madson, B. Mirante, K. Clark, L. Font, S. Korbey, T.N. Sager, J. Hockemeyer, C.E. Müller, Front. Biosci. 13 (2008) 3594–3605.
[16] K. Ishiwari, L.J. Madson, A.M. Farrar, S.M. Mingote, J.P. Valenta, M.D. DiGianvittorio, L.E. Frank, M. Correa, J. Hockemeyer, C.E. Müller, J.D. Salamone, Behav. Brain Res. 178 (2007) 190–199.
[17] A.M. Farrar, M. Pereira, F. Velasco, J. Hockemeyer, C.E. Müller, J. Salamone, Psychopharmacology 191 (2007) 579–586.
[18] C.E. Müller, S. Ferré, Recent Pat. CNS Drug Discov. 2 (2007) 1–21.
[19] (a) O. Yuzlenko, K. Kieć-Kononowicz, Curr. Med. Chem. 13 (2006) 3609–3625; (b) C.E. Müller, K.A. Jacobson, Biochim. Biophys. Acta. 1808 (2011) 1290–1308.
[20] B.B. Fredholm (Ed.), Methylxanthines, Handbook of Experimental Pharmacology, vol. 200, Springer-Verlag, Berlin, Heidelberg, 2011 ISBN: 3642134424.
[21] W.F. Kiesman, J. Zhao, P.R. Conlon, R.C. Petter, X. Jin, G. Smits, F. Lutterodt, G. Sullivan, J. Linden, Bioorg. Med. Chem. 14 (2006) 3654–3661.
[22] R. Sauer, J. Maurinsh, U. Reith, F. Fülle, N. K-Klotz, C.E. Müller, J. Med. Chem. 43 (2000) 440–448.
[23] M. Yang, D. Soohoo, S. Soelaiman, R. Kalla, J. Zablocki, N. Chu, K. Leung, L. Yao, I. Diamond, L. Belardinelli, J.C. Shryock, Naunyn-Schmiedeberg's Arch. Pharmacol. 375 (2007) 133–144.
[24] E. Ongini, A. Monopoli, B. Cacciari, P.G. Baraldi, Farmaco 56 (2001) 87–90.
[25] T.N. Chase, F. Bibbiani, W. Bara-Jimenez, T. Dimitrowa, J.D. Oh-Lee, Neurology 61 (2003) 107–111.
[26] S.S. Wu, S.J. Frucht, CNS Drugs 19 (2005) 723–743.
[27] K. Kieć-Kononowicz, A. Drabczyńska, E. Pękala, B. Michalak, C.E. Müller, B. Schumacher, J. Karolak-Wojciechowska, H. Duddeck, S. Rockitt, R. Wartchow, Pure Appl. Chem. 73 (2001) 1411–1420.
[28] A. Drabczyńska, B. Schumacher, C.E. Müller, J. Karolak-Wojciechowska, B. Michalak, E. Pękala, K. Kieć-Kononowicz, Eur. J. Med. Chem. 38 (2003) 397–402.
[29] A. Drabczyńska, C.E. Müller, B. Schumacher, S. Hinz, J. Karolak-Wojciechowska, B. Michalak, E. Pękala, K. Kieć-Kononowicz, Bioorg. Med. Chem. 12 (2004) 4895–4908.
[30] A. Drabczyńska, C.E. Müller, S.K. Lacher, B. Schumacher, J. Karolak-Wojciechowska, A. Nasal, P. Kawczak, O. Yuzlenko, K. Kieć-Kononowicz, Bioorg. Med. Chem. 14 (2006) 7258–7281.
[31] A. Drabczyńska, C.E. Müller, J. Karolak-Wojciechowska, B. Schumacher, A. Schiedel, O. Yuzlenko, K. Kieć-Kononowicz, Bioorg. Med. Chem. 15 (2007) 5003–5017.
[32] A. Drabczyńska, C.E. Müller, A. Schiedel, B. Schumacher, J. Karolak-Wojciechowska, A. Fruziński, W. Zobnina, O. Yuzlenko, K. Kieć-Kononowicz, Bioorg. Med. Chem. 15 (2007) 6956–6974.
[33] S. Rockitt, R. Wartchow, H. Duddeck, A. Drabczyńska, K. Kieć-Kononowicz, Z. Naturforsch. 56B (2001) 319–324.
[34] M. Pawłowski, A. Drabczyńska, M. Gorczyca, D. Malec, J. Modzelewski, Acta Polon. Pharm.-Drug Res. 51 (1994) 385–391.
[35] M. Eckstein, Dissert. Pharm. 14 (1962) 425–434.
[36] F. Bergmann, S. Dickstein, J. Am. Chem. Soc. 77 (1955) 691.
[37] A. Rybár, K. Antoš, Collect. Czech. Chem. Commun. 35 (1970) 1415–1425.
[38] G.R. Desiraju, T. Steiner, The Weak Hydrogen Bond in Structural Chemistry and Biology. Oxford University Press, Oxford, 1999.
[39] G.R. Desiraju, J. Hulliger, Curr. Opin. Solid State Mater. Sci. 5 (2001) 105–115.
[40] G.R. Desiraju, Acc. Chem. Res. 35 (2002) 565–573.
[41] R.P. Sijbesma, E.W. Meijer, Chem. Commun. (2003) 5–16.
[42] F.F. Awwadi, R.D. Willett, B. Twamley, J. Mol. Struct. 918 (2009) 116–122.
[43] J.-M. Lehn, Angew. Chem. 27 (1988) 89–112.
[44] K.-N. Klotz, I. Hessling, J. Hegler, C. Owman, B. Kull, B.B. Fredholm, M.J. Lohse, Naunyn-Schmiedeberg's Arch. Pharmacol. 357 (1998) 1–9.
[45] C.E. Müller, J. Maurinsh, R. Sauer, Eur. J. Pharm. Sci. 10 (2000) 259–265.
[46] X.-D. Ji, K.A. Jacobson, Drug Des. Discov. 16 (1999) 217–226.
[47] T. Borrmann, S. Hinz, D.C.G. Bertarelli, W. Li, N.C. Florin, A.B. Scheiff, C.E. Müller, J. Med. Chem. 52 (2009) 3994–4006.
[48] C.E. Müller, M. Diekmann, M. Thorand, V. Ozola, Bioorg. Med. Chem. Lett. 12 (2002) 501–503.
[49] D.C.G. Bertarelli, M. Diekmann, A.M. Hayallah, D. Rüsing, J. Iqbal, B. Preiss, E.J. Verspohl, C.E. Müller, Purinergic Signal. 2 (2006) 559–571.
[50] Z.G. Gao, A.P. IJzerman, Biochem. Pharmacol. 60 (2000) 669–676.
[51] P.J. van Galen, A.H. van Bergen, C. Gallo-Rodriguez, N. Melman, M.E. Olah, A.P. IJzerman, G.L. Stiles, K.A. Jacobson, Mol. Pharmacol. 45 (1994) 1101–1111.
[52] H.J. Kupferberg, Epilepsia 30 (1989) S51–S56.
[53] A. Le Tiran, J.P. Stables, H. Kohn, J. Med. Chem. 45 (2002) 4762–4773.
[54] D. Mulzac, K. Scott, Epilepsia 34 (1993) 1141–1146.
[55] S. McGaraughty, M. Cowart, M.F. Jarvis, R.F. Berman, Curr. Top. Med. Chem. 5 (2005) 43–58.
[56] CAChe Worksystem Pro 6.1. CAChe Group, Fujitsu Limited, Japan, 2003.
[57] A.K. Ghose, A. Pritchett, G.M. Crippen, J. Comput. Chem. 9 (1988) 80–90.
[58] A. Golbraikh, M. Shen, Z. Xiao, Y.D. Xiao, K.H. Lee, A. Tropsha, J. Comput.-Aided Mol. Des. 17 (2003) 241–253.
[59] L. He, P.C. Jurs, J. Mol. Graph. Model. 23 (2005) 503–523.
[60] CAChe Worksystem Pro 7.6. CAChe Group, Fujitsu Limited, Japan, 2007.
[61] A. Golbraikh, A. Tropsha, J. Mol. Graph. Model. 20 (2002) 269–276.
[62] G.M. Sheldrick, SHELXTL PC^{MT}. Siemens Analytical X-Ray Instruments Inc., Madison, Wisconsin, USA, 1990.
[63] G.M. Sheldrick, SHELXTL-97. A FORTRAN-77 Program for the Refinement of Crystal Structures from Diffraction Data. University of Göttingen, Germany, 1997.
[64] L. Yan, D.C.G. Bertarelli, A.M. Hayallah, H. Meyer, K.-N. Klotz, C.E. Müller, J. Med. Chem. 49 (2006) 4384–4391.
[65] J. Bulicz, D.C.G. Bertarelli, D. Baumert, F. Fülle, C.E. Müller, D. Heber, Bioorg. Med. Chem. 14 (2006) 2837–2849.
[66] C. Nordstedt, B.B. Fredholm, Anal. Biochem. 189 (1990) 231–234.